Energy conversion regions as observed by Cluster in the plasma sheet

M. Hamrin,[1] O. Marghitu,[2] P. Norqvist,[1] S. Buchert,[3] M. André,[3] B. Klecker,[4] L. M. Kistler,[5] and I. Dandouras[6]

Received 20 December 2010; revised 15 April 2011; accepted 20 April 2011; published 21 July 2011.

[1] In this article we present a review of recent studies of observations of localized energy conversion regions (ECRs) observed by Cluster in the plasma sheet at altitudes of 15–20R_E. By examining variations in the power density, $\mathbf{E} \cdot \mathbf{J}$, where $\mathbf{E}$ is the electric field and $\mathbf{J}$ is the current density, we show that the plasma sheet exhibits a high level of fine structure. Approximately three times as many concentrated load regions (CLRs) ($\mathbf{E} \cdot \mathbf{J} > 0$) as concentrated generator regions (CGRs) ($\mathbf{E} \cdot \mathbf{J} < 0$) are identified, confirming the average load character of the plasma sheet. Some ECRs are found to relate to auroral activity. While ECRs are relevant for the energy conversion between the electromagnetic field and the particles, bursty bulk flows (BBFs) play a central role for the energy transfer in the plasma sheet. We show that ECRs and BBFs are likely to be related, although details of this relationship are yet to be explored. The plasma sheet energy conversion increases rather simultaneously with increasing geomagnetic activity in both CLRs and CGRs. Consistent with large-scale magnetotail simulations, most of the observed ECRs appear to be rather stationary in space but varying in time. We estimate that the ECR lifetime and scale size are a few minutes and a few R_E, respectively. It is conceivable that ECRs rise and vanish locally in significant regions of the plasma sheet, possibly oscillating between load and generator character, while some energy is transmitted as Poynting flux to the ionosphere.

Citation: Hamrin, M., O. Marghitu, P. Norqvist, S. Buchert, M. André, B. Klecker, L. M. Kistler, and I. Dandouras (2011), Energy conversion regions as observed by Cluster in the plasma sheet, *J. Geophys. Res.*, *116*, A00K08, doi:10.1029/2010JA016383.

1. Introduction

[2] There are many unsolved problems related to the energy budget of the Earth's magnetosphere. Bright auroral forms, which perhaps are the most spectacular phenomena that regularly can be observed on the dark night sky, is an apparent proof of the existence of a set of complicated processes involving the energy conversion and transfer in the magnetosphere, from the solar wind and to the auroral ionosphere. Intriguing problems regarding the magnetospheric energy budget concern issues such as the energy input into the magnetosphere [e.g., *Koskinen and Tanskanen*, 2002], the nature of tail reconnection [e.g., *Sharma et al.*, 2008], the location of the auroral generator [e.g., *Rostoker*, 1999], the role of the magnetosphere-ionosphere (M-I) coupling [e.g., *Mauk et al.*, 2002], as well as the high-speed flows and the energy transport in the M-I system [e.g., *Sergeev*, 2004]. Large amounts of energy are released during substorms, and auroral arcs in the ionosphere are connected via magnetic field-aligned currents to the nightside magnetosphere in the auroral current circuit. Even though auroral processes have been investigated for a long time, our understanding of the detailed mechanisms behind the generation and evolution of auroras is still rather fragmented and uncertain. For example, where are the auroral generators explicitly located and what are their properties?

[3] Within the magnetosphere, energy is mediated between different forms. In load regions, magnetic pressure and tension accelerate the plasma, and electromagnetic energy is converted into kinetic energy (plasma bulk and thermal). The process is reversed in generator regions. The plasma sheet is known to play a central role for the energy budget of the Earth's magnetosphere [e.g., *Lyons*, 2000; *Koskinen and Tanskanen*, 2002; *Pulkkinen et al.*, 2003]. During substorms, the amount of energy dissipated in the plasma sheet (in the form of plasmoid ejection and ion heating) is comparable to the ring current dissipation, auroral Joule heating and charged particle precipitation into the ionosphere [*Ieda et al.*, 1998; *Slavin et al.*, 1993]. Since the plasma sheet maps to the nightside auroral ionosphere, various regions in

[1]Department of Physics, Umeå University, Umeå, Sweden.
[2]Institute for Space Sciences, Bucharest, Romania.
[3]Swedish Institute of Space Physics, Uppsala, Sweden.
[4]Max-Planck-Institut für Extraterrestrische Physik, Garching, Germany.
[5]Space Science Center, Institute for the Study of Earth, Oceans, and Space, University of New Hampshire, Durham, New Hampshire, USA.
[6]CESR-CNRS, Toulouse, France.

0148-0227/11/2010JA016383

the plasma sheet have been suggested to host auroral generators, for example, the low-latitude boundary layer and the plasma sheet boundary layer (PSBL). However, even though the plasma sheet on the average behaves as a load due to the dawn to dusk electric field and cross-tail current, it is a complicated plasma regime comprising both generators and loads [e.g., *Birn and Hesse*, 2005; *Marghitu et al.*, 2010; *Hamrin et al.*, 2009a].

[4] The processes in the plasma sheet of course only constitute a few links in the long chain of processes controlling the energy conversion and transfer in the Earth's magnetosphere. The primary energy source for the magnetospheric energy budget is solar wind kinetic energy, which can be transferred into the magnetosphere by means of magnetopause reconnection. Indeed, reconnection is one key process at several stages of the magnetospheric energy budget [e.g., *Paschmann*, 2008]. Not only does it regulate the solar wind energy and momentum input at the magnetopause [*Paschmann et al.*, 1979], but it also controls the substorm magnetic energy release in the Earth's magnetotail [e.g., *Fujimoto et al.*, 2001].

[5] The primary magnetospheric convection is believed to be controlled by the Dungey cycle with dayside magnetopause reconnection in combination with a reconnection X line in the distant magnetotail [*Dungey*, 1961]. The corresponding cross-tail electric field and current systems are the cause for the average load behavior of the plasma sheet. During substorm expansion, another reconnection site is expected to form as a near-Earth neutral line (NENL) 20–30R_E downtail in the plasma sheet [e.g., *Nagai et al.*, 2001]. According to recent investigations, the plasma sheet energy conversion between magnetic energy on the one hand, and bulk kinetic and thermal energy on the other, may be associated with multiple, small-scale, and intermittent reconnection processes [e.g., *Treumann et al.*, 2009] in a turbulent plasma environment.

[6] The solar wind kinetic energy powers generators located at the magnetopause. Generated electromagnetic energy is partially stored in the tail magnetic field, particularly the lobes. Tail reconnection and perhaps also other processes, e.g., resistivity, then convert the electromagnetic energy into kinetic and thermal energy. A popular notion is hence that the aurora is powered by the solar wind. Indeed, an open magnetopause at a few R_E tailward of the dawn-dusk meridian has been observed to act like a generator with a significant component of the magnetic tension directed against the solar wind flow, thus producing Poynting flux pointing into the magnetotail [*Rosenqvist et al.*, 2006]. According to *Rosenqvist et al.* [2006], estimates of the global Joule heating in the Earth's upper atmosphere and ionosphere during an intense storm amounted to roughly 35% of the power extracted from the solar wind at the magnetopause. However, under normal circumstances we can expect that a considerable fraction of the electromagnetic power dissipated in the ionosphere is not directly generated at the magnetopause, since nightside auroral field lines on the equatorward edge of the oval, and at least up into the central part, map from the ionosphere rather into the tail region (specifically the plasma sheet).

[7] The energy stored in the tail magnetic field is converted into kinetic energy at rather localized acceleration sites, and plasma is transported toward the Earth, or tailward into the interplanetary plasma. These high-speed flows can be manifested as bursty bulk flows (BBFs) and other sporadic and intermittent phenomena [e.g., *Scholer et al.*, 1984; *Angelopoulos et al.*, 1992; *Chen and Wolf*, 1993; *Angelopoulos et al.*, 2002]. For example, the large substorm current wedge is believed to be caused by the braking and diversion of earthward directed flows closer to the inner boundary of the plasma sheet, resulting in the generation of electromagnetic power, which eventually can power the aurora [*Wygant et al.*, 2000] as well as cause ionospheric Joule heating.

[8] Alongside the process of reconnection, high-speed flows in the plasma sheet is hence another important key issue involved in the magnetospheric energy budget. Such flows are observed in various regions of the magnetotail, both in the central plasma sheet (CPS) and in the PSBL. However, the characteristics of the high-speed flows differ generally between the regions. In the CPS, the high-speed flows are generally bulk flows which are (quasi-) perpendicular to the ambient magnetic field, with GSM V_x being the dominant velocity component, and V_y occasionally substantial [*Angelopoulos et al.*, 1994]. In the PSBL, on the other hand, the high-speed flows can usually be characterized as field-aligned beams [*Nakamura et al.*, 1992; *Petrukovich et al.*, 2001].

[9] The concept of BBFs was first introduced by *Angelopoulos et al.* [1992] who investigated the occurrence of bursty bulk flows in the inner CPS, as characterized by a large plasma $\beta > 0.5$. Typically, BBFs correspond to bursty high-speed flow events observed on a 10 min time scale, and composed of individual high-speed flow burst ($\gtrsim$400 km/s) on shorter time scales, of the order of tens of seconds [*Angelopoulos et al.*, 1992, 1994]. Subsequently, field aligned burst have been observed also in lower β plasmas outside the PSBL, i.e., where $\beta < 0.5$ [*Raj et al.*, 2002]. Therefore, it is practical to include also the field aligned beams into the definition of BBFs [*Snekvik et al.*, 2007]. Observational investigations have shown that BBFs often are associated with ion heating and local magnetic field dipolarization (magnetic pileup) at the front or stopping region, corresponding to a locally enhanced northward B_z [e.g., *Fairfield et al.*, 1999; *Nakamura et al.*, 2005a; *Sergeev et al.*, 1996b]. The BBFs are likely to show a reduction in the plasma pressure initially, but evolving toward values comparable to, or sometimes even greater, than the surrounding medium [*Chen and Wolf*, 1999].

[10] A possible theoretical explanation for BBFs comes from the theory of plasma bubbles. As compared to the surrounding plasma, bubbles are depleted flux tubes with decreased entropy, and increased earthward propagation velocity (possibly propelled by a magnetic buoyancy force, related to the interchange instability) [*Pontius and Wolf*, 1990; *Chen and Wolf*, 1993, 1999]. Details of the propagation of a plasma bubble have been investigated in a 3-D MHD simulation by *Birn et al.* [2004]. Bubbles are expected to be created by reconnection processes and/or other processes in the plasma sheet [e.g., *Sergeev*, 2004], and simulations indicate that the tailward ejection of plasmoids from a reconnection site also can be explained by bubble theory [*Sitnov et al.*, 2005].

[11] The plasma bubble cannot support as much diamagnetic, curvature and drift current as the surrounding plasma.

Current continuity is instead maintained by field-aligned currents at the sides of the flux tube. As shown by *Birn et al.* [2004], flow vortices appear at the flanks of the bubble, twisting the magnetic field, and causing a downward (upward) field-aligned current at the dawnside (duskside) flank, and forming a local wedge like current system [e.g., *Chen and Wolf*, 1993, 1999; *Sergeev et al.*, 1996a; *Birn and Hesse*, 1996; *Birn et al.*, 1999, 2004; *Snekvik et al.*, 2007; *Zhang et al.*, 2009]. A return plasma flow may occur at the flanks of the bubble, and the corresponding shear against the plasma flow in the bubble main channel may also be involved in the generation of the field-aligned currents [e.g., *Chen and Wolf*, 1999; *Kauristie et al.*, 2000; *Birn et al.*, 2004; *Keiling et al.*, 2009; *Ohtani et al.*, 2009; *Walsh et al.*, 2009; *Panov et al.*, 2010a, 2010b; *Birn et al.*, 2011; *Ge et al.*, 2011; *Pitkänen et al.*, 2011].

[12] High-speed flows in the plasma sheet, such as BBFs and bubbles, are central ingredients in magnetospheric energy budget. (Note that we will use the denomination BBF for high-speed plasma flows throughout the rest of the article, independently of the detailed character of the flows.) BBFs are believed to play a major role for magnetic flux, mass, and energy transport in the plasma sheet [e.g., *Angelopoulos et al.*, 1992, 1994, 1999; *Sergeev et al.* 1996b; *Schödel et al.*, 2001], and it has been showed that BBFs have the largest capability of transporting energy during the substorm expansion phase, as compared to the growth and recovery phases [*YuDuan et al.*, 2010]. In the literature there are many reports of the relation between BBFs and auroral phenomena at the ionospheric end of the M-I coupling system, e.g., auroral expansions, localized brightenings, and auroral streamers [e.g., *Fairfield et al.*, 1999; *Lyons et al.*, 1999; *Ieda et al.*, 2001; *Sergeev et al.*, 2001; *Nakamura et al.*, 2001a, 2001b, 2005b; *Miyashita et al.*, 2003; *Forsyth et al.*, 2008].

[13] The multispacecraft Cluster mission is favorable for observational investigations of the energy conversion in the plasma sheet. The reason is that a minimum of four simultaneous measurements of the magnetic field is needed for estimating the full current density. Load and generator regions can be identified by analyzing observations of the power density $\mathbf{E} \cdot \mathbf{J}$, where $\mathbf{E}$ is the electric field and $\mathbf{J}$ the current density. Local conversion from kinetic to electromagnetic energy occurs in generator regions where $\mathbf{E} \cdot \mathbf{J} < 0$, and the process is reversed in load regions where $\mathbf{E} \cdot \mathbf{J} > 0$. Using plasma sheet Cluster data we present in this article a review of recent observations of localized energy conversion regions (ECRs), and we discuss the high level of fine structure in the plasma sheet energy conversion. To our knowledge, the first experimental evidences for plasma sheet ECRs in the form of generator regions were obtained from Cluster data by *Marghitu et al.* [2006] and *Hamrin et al.* [2006].

[14] There are reasons to expect that there is a relationship between ECRs and the energy transfer in the form of BBFs in the plasma sheet. In a statistical investigation, *Morioka et al.* [2010] showed that the generation of field-aligned currents and accelerated auroral electrons in the auroral current circuit is tightly coupled to flow burst in the plasma sheet. Indeed, 65% of the flow bursts observed from Geotail data appeared to correspond to the generation of auroral kilometric radiation (AKR) in the auroral acceleration region within the M-I coupling region [*Morioka et al.*, 2010]. Moreover, recent investigations by *Marghitu et al.* [2010] and O. Marghitu et al. (manuscript in preparation, 2011) suggest that ECRs are often associated with BBFs, even though there are occasions where ECRs are observed without any strong and distinct signatures in the ion velocity data. This could for example indicate that other processes dominate, or that the Cluster spacecraft miss the main plasma flow. Detailed investigations of the relation between BBFs and ECRs are needed to resolve this issue.

[15] In this article we do not intend to achieve a complete review of all energy conversion and transfer processes relevant for the plasma sheet and the M-I coupling. Instead, the main focus is on summarizing the observations of the ECRs and hint to their possible relation to BBFs. However, it should be noted that we have observed ECRs during varying geomagnetic and/or substorm activities, while many investigations concerning BBFs are related to disturbed times, even though there are exceptions [e.g., *Pitkänen et al.*, 2011]. Figure 1 shows a schematic overview of some important energy conversion processes relevant for the Earth's plasma sheet.

1.1. Theoretical Motivation

[16] The physical interpretation of the power density, $\mathbf{E} \cdot \mathbf{J}$, is that it corresponds to the amount of energy (per unit volume and per unit time) converted between its electromagnetic and kinetic forms. This can be verified from the Poynting theorem (i.e., equation of conservation of the electromagnetic energy)

$$\frac{\partial W_{EM}}{\partial t} = -\nabla \cdot \mathbf{S} - \mathbf{E} \cdot \mathbf{J}, \tag{1}$$

where W_{EM} is the electromagnetic energy density, and $\mathbf{S}$ is the Poynting vector. When $\mathbf{E} \cdot \mathbf{J} < 0$, energy is transferred from the particles to the fields, and the electromagnetic energy density increases. Similarly, the electromagnetic energy density decreases when $\mathbf{E} \cdot \mathbf{J} > 0$, and energy is transferred from the fields to the particles.

[17] The relation of $\mathbf{E} \cdot \mathbf{J}$ as a mediator between the electromagnetic and kinetic energy forms can also be verified from ideal magnetohydrodynamic (MHD) theory (note that heat flux is neglected in MHD). Multiplying the one-fluid equation of motion

$$\rho \frac{d\mathbf{v}}{dt} = \mathbf{J} \times \mathbf{B} - \nabla p \tag{2}$$

with the plasma bulk velocity, $\mathbf{v}$, and using the continuity equation

$$\frac{\partial \rho}{\partial t} = -\nabla \cdot \rho \mathbf{v}, \tag{3}$$

we obtain an equation for the energy conservation of the bulk motion

$$\frac{\partial W_k}{\partial t} = -\nabla \cdot (W_k \mathbf{v}) - \mathbf{v} \cdot \nabla p + \mathbf{E} \cdot \mathbf{J}, \tag{4}$$

where we have assumed a scalar pressure p. The time variation of the bulk kinetic energy density, $W_k = \rho v^2/2$, is

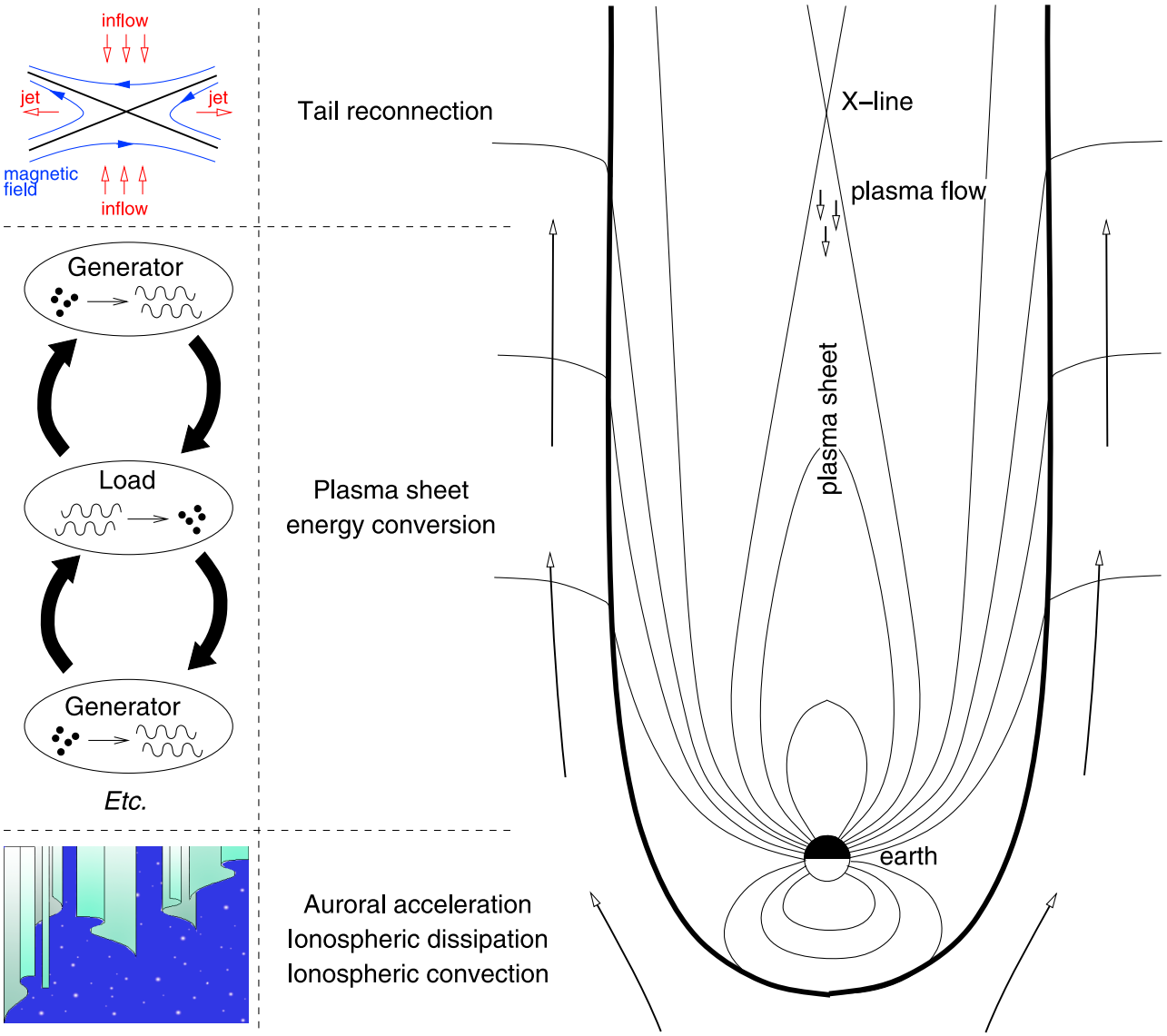

Figure 1. Schematic overview of some important energy conversion processes relevant for the Earth's plasma sheet. Tail reconnection causes high-speed plasma flows, e.g., BBFs or plasma bubbles, toward the Earth. These flows can power generators where kinetic energy is transformed into electromagnetic energy. The process is reversed in load regions where energy is transferred back from the fields to the particles. One might expect that at least some of the energy is locally converted back and forth between the particles and the fields in localized load and generator regions in the plasma sheet. Some energy is also transported to the ionosphere, where it powers auroral related processes.

expressed in the left hand side of the equation. The right hand side corresponds to its source terms, i.e., the divergence of the bulk kinetic energy flux ($-\nabla \cdot (W_k \mathbf{v})$), the work done by the pressure forces on the plasma ($-\nabla p \cdot \mathbf{v}$), and the work done by the electromagnetic forces on the plasma ($\mathbf{E} \cdot \mathbf{J}$). When $\mathbf{E} \cdot \mathbf{J} > 0$, the kinetic energy density increases since work is done on the plasma by electromagnetic forces. On the other hand, when $\mathbf{E} \cdot \mathbf{J} < 0$ the particles are losing energy to the field, corresponding to a decrease in kinetic energy density. Practically, what determines the sign of the power density is the acceleration or deceleration of the plasma element by magnetic pressure and tension (the Lorenz force), i.e., $\mathbf{J} \times \mathbf{B}$ versus $-\nabla p$ in the one-fluid MHD equation of motion (equation (2)).

[18] In Figure 2 we present a sketch of a BBF in the equatorial plane. The BBF is represented by the earthward plasma flow (light green) together with flow braking and diversion closer to the inner plasma sheet boundary. Possible BBF return flows are also indicated by the green dashed arrows [*Chen and Wolf*, 1999; *Kauristie et al.*, 2000; *Birn et al.*, 2004; *Keiling et al.*, 2009; *Ohtani et al.*, 2009; *Walsh et al.*, *Panov et al.*, 2010a, 2010b]. The shear and twisting of the magnetic field at the flanks of the BBF causes field-aligned currents (magenta) connecting to the auroral iono-

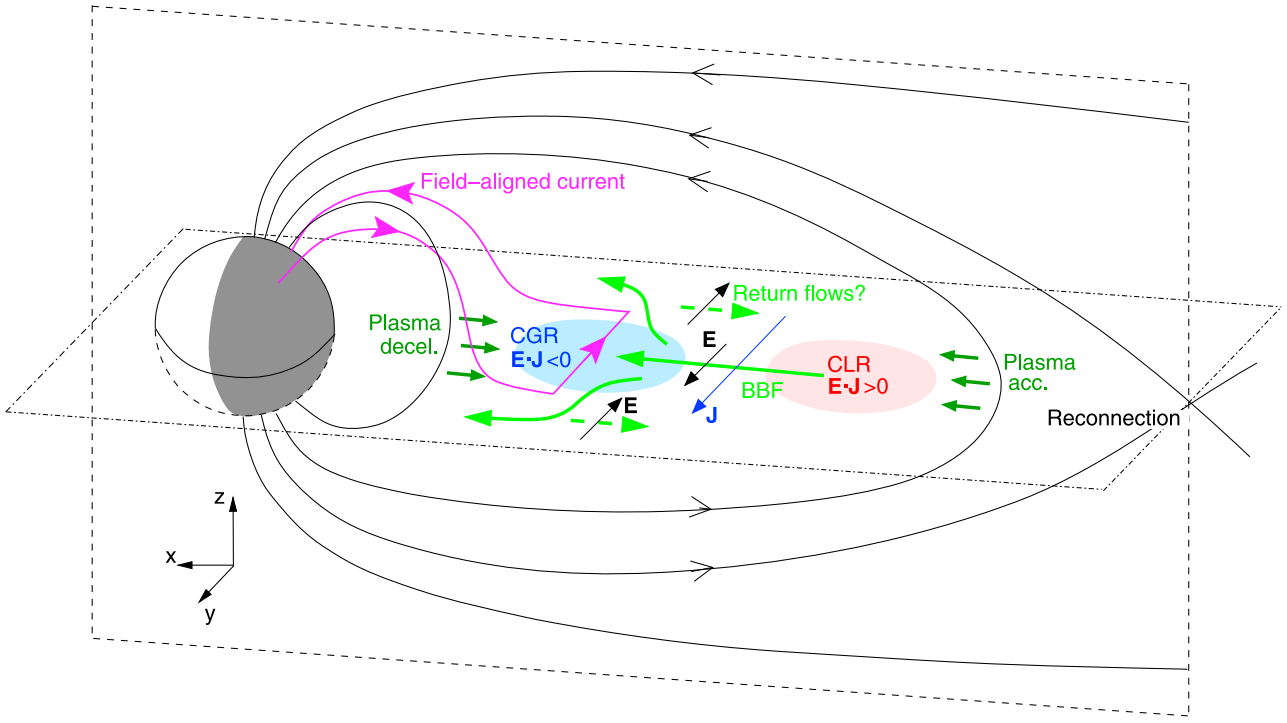

Figure 2. Schematic overview of the relation between ECRs and BBFs. See the text for details.

sphere [cf. *Birn et al.*, 2004]. In this simplified picture, plasma is accelerated by the magnetic pressure and tension to the right side of Figure 2, and decelerated to the left (dark green arrows).

[19] Assuming a simplified magnetic field direction as shown in Figure 2, in the main BBF flow channel we see that the electric field (black) is directed toward dusk (positive y), and in the return flow it is directed toward dawn. However, in a general case with a more turbulent plasma flow, and more complicated magnetic field configurations, the electric field direction can vary.

[20] Depending on the direction of the cross-tail current (in positive or negative y in Figure 2) in relation to the electric field, load and generator regions appear. The typical dawn to dusk cross-tail current is indicated with the blue arrow. Assuming field-aligned currents toward the northern ionosphere and current closure across the main region of the BBF (magenta), the power density is negative toward the front of the BBF, i.e., a CGR. In Figure 2 this would correspond to the current wedge with its reduction and diversion of the ambient cross-tail current. Another scenario is that CLRs and CGRs are associated with the central BBF channel and the return flows, respectively. We also refer to *Birn et al.* [1999] and *Zhang et al.* [2011] for examples of various possible current systems in the magnetotail (not only closing in the ionosphere but also within the magnetosphere). For example, as discussed by *Juusola et al.* [2009], if the ionospheric conductivity is low (e.g., during low geomagnetic activity), tail current systems may also close more locally in the magnetosphere. To simplify the sketch, note that we only highlight one CLR (red) and one CGR (blue) in Figure 2. However, in a more general case one may expect several conversions back and forth between electromagnetic and kinetic energy forms in the plasma sheet.

[21] Note that equation (2) only is valid for ideal MHD, where $\mathbf{E} = -\mathbf{v} \times \mathbf{B}$, while additional work terms add on the right hand side in nonideal cases. According to section 2, the electric field can be estimated indirectly from particle moments through $\mathbf{v} \times \mathbf{B}$, or it can be obtained from direct field measurements. As shown by *Hamrin et al.* [2009a], there is a clear correlation between $E_y J_y$ as obtained from the particle moments and from direct measurements. This implies that the ideal MHD assumption is relevant for investigations of Cluster plasma sheet ECRs.

1.2. Frame of Reference

[22] When investigating localized energy conversion by using the power density, the choice of the reference frame is utterly important. The current density is invariant under nonrelativistic coordinate transformations, but the electric field is not [*Barger and Olsson*, 1987]. Consequently, the power density is not coordinate invariant, and it is possible to obtain different values (or even different signs) of the power density by changing the frame of reference.

[23] A suitable choice would be to use the same frame of reference for all tightly interacting loads and generators within a defined system. In the system of the auroral magnetosphere, a few basic load and generator regions can be identified: (1) the reconnection X line load, (2) load and generator regions within the highly structured plasma sheet (possibly oscillating energy between its kinetic and electromagnetic forms), (3) the load in the auroral acceleration region, and (4) the load corresponding to the ionospheric Joule heating. When investigating local energy conversion in the plasma sheet load and generator regions, it is appropriate to use the reference frame of the Joule dissipation, approximately the frame of the neutral winds. This frame moves with respect to GSE or GSM, however, the associ-

Table 1. Overview of the Events Included in the Database for the Individual Years (2001, 2002, and 2004) and for All 3 Years Together (Last Row)[a]

	PS Passages		CLR		CGR			RAND-LG		Ratio N_L/N_G		
Year	N_{PS}	ΔT_{PS}	N_L	ΔT_L	N_G	ΔT_G	CLR+CGR $N_{L+G}/\Delta T_{PS}$	N_L	N_G	ECR	RAND	Cluster Scale ΔS
2001	85	660 h	110	12 h	24	1.5 h	0.20 h^{-1}	577	464	4.6	1.2	1500 km
2002	68	1000 h	173	17 h	60	3.2 h	0.23 h^{-1}	450	275	2.9	1.6	4000 km
2004	67	1070 h	145	11 h	43	1.9 h	0.18 h^{-1}	440	258	3.4	1.7	1000 km
All years	220	2730 h	555	40 h	127	6.6 h	0.20 h^{-1}	1467	997	3.4	1.5	1000–4000 km

[a]The second and third columns contain the number of Cluster plasma sheet passages and the available hours of plasma sheet data. The fourth to seventh columns contain the number of CLRs, the accumulated time extent of the CLRs, the number of CGRs, and the accumulated time extent of the CGRs, respectively. The total number of ECRs (CLRs + CGRs) per available hour of Cluster plasma sheet data is presented in the eighth column. The ninth and tenth columns contain the number of RAND-Ls and RAND-Gs, respectively. The ratio between the number of load and generators among the ECRs and the RANDs (i.e., CLRs/CGRs and RAND-Ls/RAND-Gs) are shown in the eleventh and twelfth columns. In the last column, information on the characteristic scale size of the Cluster tetrahedron can be found. Adapted after *Hamrin et al.* [2010].

ated motional electric field is negligible, less than 30 μV/m. Hence a suitable choice when investigating plasma sheet load and generator regions involves the GSE and the GSM frames of reference [*Marghitu et al.*, 2006].

1.3. Observational Investigations

[24] Observational investigations of the power density are complicated due to experimental limitations. In many cases, the expected power density in plasma sheet generator and load regions is of the order of 1 to a few pW/m^3 [*Birn and Hesse*, 2005; *Marghitu et al.*, 2006]. This implies electric and magnetic field measurements often close to the detection limits of the available instruments.

[25] In the literature, there is a lack of in situ investigations of the plasma sheet energy conversion. The four spacecraft Cluster mission offers for the first time suitable conditions for detailed observational investigations of the plasma sheet energy conversion, via the evaluation of the power density. Especially, estimating the full current density requires multispacecraft missions such as Cluster, with at least four simultaneous measurements of the magnetic field.

[26] In this article we give a comprehensive overview of Cluster observations of localized energy conversion in the plasma sheet. The reviewed investigations are based on Cluster data from the summer and fall half-years of 2001, 2002, and 2004 when the spacecraft were probing the plasma sheet at altitudes of 15–20R_E. In section 2 we present the method by which the ECRs have been identified from the Cluster power density data. General properties of the ECRs, such as occurrence frequency, location, power density strength, lifetime, and scale size are addressed in section 3. In section 2 we show that the plasma sheet energy conversion increases with increasing geomagnetic activity, and in section 5 we show that at least a fraction of the observed ECRs at Cluster altitudes are related to lower-altitude auroral activity. In section 6, the overall results are summarized.

2. Instrumentation and Method

[27] The Cluster mission consists of four identical spacecraft, which were launched in 2000 into a polar orbit with orbital period of about 57 h, and with apogee and perigee at about 18R_E and 3R_E, respectively. The spacecraft fly in a tetrahedral formation, and spin with a period of approximately 4 s around an axis almost parallel to the GSE z direction. For a discussion of the Cluster mission and instruments [see *Escoubet et al.*, 2001, and references therein].

[28] The primary data set used in this survey article is plasma sheet power density data, $\mathbf{E} \cdot \mathbf{J}$, obtained from Cluster in 2001, 2002, and 2004. Data from 2003, as well as 2005 and later years, are not included in the present investigations due to unsatisfactory spacecraft configuration, and for later years also due to instrumental degradings (cf. *Hamrin et al.* [2010] for a discussion of the data quality over the years). For 2005 and later years, the satellites were in a multiscale mode which implies that the configuration was not suitable for computing gradients, i.e., the current density. In 2003 the Cluster tetrahedron scale size was comparable to or smaller than the proton gyroradii. Kinetic effects might hence be important for the interpretation of the 2003 data, and this is outside the scope of the present article.

[29] The full current density vector, $\mathbf{J}$, is calculated from $\nabla \times \mathbf{B}/\mu_0$ (neglecting the displacement current) by using the curlometer method [*Robert et al.*, 1998; *Dunlop et al.*, 2002]. The size and shape of the Cluster tetrahedron affect the curlometer estimate, and current density structures smaller than the characteristic size of the tetrahedron cannot generally be resolved with the curlometer. In 2001, 2002, and 2004, the shape of the Cluster tetrahedron was optimal (approximately equilateral tetrahedron) for obtaining current density estimates within the plasma sheet. The characteristic size of the tetrahedron varied over the years between ~1000 km and ~4000 km (see Table 1). With an average proton gyroradius of a few hundred km at Cluster altitudes, this corresponds to tetrahedron scale sizes generally larger then the ion scales.

[30] The electric field, $\mathbf{E}$, is derived from ion measurements obtained by the two Cluster CIS sensors, CODIF and HIA, on the assumption that the $\mathbf{E} \times \mathbf{B}$ drift is dominant. The resulting power density represents actually just the normal contribution, $\mathbf{E}_\perp \cdot \mathbf{J}_\perp$, while the field-aligned contribution, $\mathbf{E}_\parallel \cdot \mathbf{J}_\parallel$, cannot be computed based on Cluster data. However, considering the time scale of our measurements of about 10 s ($\gtrsim$4 s), this contribution is likely to be negligible most of the time. Since the maximum time resolution of ion moments from CIS is 4 s, the maximum resolution of the power density is also 4 s. Faster variations in the plasma sheet energy conversion cannot be resolved in our investigations. Electric field measurements from the electric fields and waves experiment (EFW) are used for cross-checking our results. The EDI (electron drift) instrument is also designed to measure the electric field, but this instrument is rarely

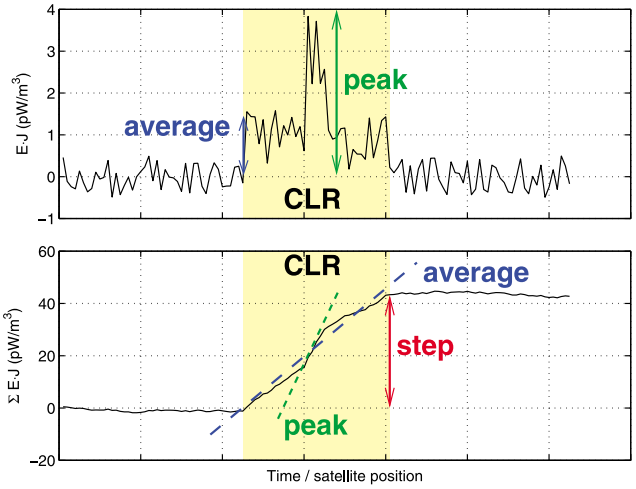

Figure 3. Schematic CLR highlighted in yellow. (top) The power density and (bottom) its accumulated value (calculated as a cumulative sum) along the satellite path. The quantities "peak" and "average" correspond to the maximum and average value of the time series of the power density and hence the maximum and average slope in the integrated power density. A CGR behaves similarly but with $\mathbf{E} \cdot \mathbf{J} < 0$ [from *Hamrin et al.*, 2010].

operational in the plasma sheet due to weak magnetic field strengths.

[31] Since the current density can be interpreted as an average value over the Cluster tetrahedron, unless otherwise stated, in our investigations we also average the electric field over the available instruments before computing the power density. This average is only based on measurements from Cluster spacecraft C1, C3, and C4, since the CIS instrument on C2 was not operational during the investigated time period (2001, 2002, and 2004). CODIF was operational on C1, C3, and C4, and HIA on C1 and C3. However, CODIF on C3 suffered from a higher noise level due to a degraded particle detection efficiency. For statistical investigations using Cluster data from later years (after 2001), CODIF on C3 is therefore not included in the electric field average. Moreover, CODIF on C1 was only operational until 25 October 2004, and is thereafter replaced by HIA on C1 in the computation of the average electric field.

[32] In the investigations summarized in this article, we analyze Cluster plasma sheet data and study regions that we call energy conversion regions (ECRs), and we hint to their possible relation to BBFs. To identify an ECR, the sign of the power density is examined. Figure 3 shows a schematic sketch of a typical load region as it could be observed in the power density data. The load is highlighted in yellow, and it manifests itself as a concentrated region with $\mathbf{E} \cdot \mathbf{J} > 0$, with both peak and average power density clearly above the surrounding fluctuations, as shown in Figure 3 (top). The total amount of energy or power converted by the load can be estimated by accumulating the power density along the spacecraft path, either by time integration or by a cumulative sum. This results in a step value with physical units of either J/m^3 or W/m^3, depending on the calculation method used (integration or summing). For a load region, there is consequently a clear positive step in the accumulated power density as shown in Figure 3 (bottom). Such a region is labeled a concentrated load region (CLR). A concentrated generator region (CGR) is similar to this, but the power density is instead negative, $\mathbf{E} \cdot \mathbf{J} < 0$.

[33] Both single events studies, as well as statistical investigations, are reviewed in this article. For the statistical examinations, the event selection has been performed by an automatic selection routine, which identifies clear concentrated regions with $\mathbf{E} \cdot \mathbf{J} > 0$ and $\mathbf{E} \cdot \mathbf{J} < 0$, respectively. To be accepted by the automatic selection routine, every CLR and CGR must fulfil a set of instrumental and physical criteria to assure a reliable selection. The automatic selection routine has been tuned to avoid too noisy events. Depending on the actual method of computing of the power density, especially as including or not including data from CODIF on C3 (see above), this fine tuning has been adjusted. Note that only the most distinct ECRs are selected by the automatic routine. It is hence likely that the occurrence frequency of localized ECRs in the plasma sheet is underestimated by this procedure.

[34] When analyzing the ECR database, the results are compared with a large database of randomly selected time intervals, evenly spread within the available Cluster plasma sheet data. The aim for using this RAND database is to distinguish between the typical behavior of the ECRs and the general behavior of the plasma sheet, as well as distinguishing the ECR signatures from any noise and variability possibly present in the Cluster plasma sheet data. Depending on the observed sign of the power density within the events of the RAND database, they are sorted into two subsets, i.e., random loads (RAND-Ls) and random generators (RAND-Gs), respectively. Note that the notation CLR and CGR is reserved only for the true ECRs, which are more carefully selected by the automatic routines. A more detailed discussion of the event selection, and the interpretation of the RAND events, is discussed by *Hamrin et al.* [2009a, 2010].

3. ECR Properties

[35] In initial investigations of the plasma sheet energy conversion, Cluster data only from 2001 were used, either for single event studies [*Hamrin et al.*, 2006; *Marghitu et al.*, 2006] or for statistical surveys [*Hamrin et al.*, 2009a, 2009b; *Marghitu et al.*, 2010]. Later investigations include also Cluster plasma sheet data from 2002 and 2004 [*Hamrin et al.*, 2010]. Detailed analysis of the observed ECR properties over all years of interest is discussed by *Hamrin et al.* [2010]. Table 1 summarizes these data. Note that fewer hours of plasma sheet data are identified from 2001 than from the other years. This is caused by a reduced telemetry duty cycle until the middle of 2002.

3.1. ECR Occurrence

[36] According to Table 1, in total 134 ECRs are observed in 2001 (whereof there are 110 CLRs and 24 CGRs), 233 in 2002 (173 CLRs and 60 CGRs), and 188 in 2004 (145 CLRs and 43 CGRs). Hence, this corresponds to a general occurrence frequency of about 0.2 ECRs observed by Cluster per hour in the plasma sheet. Calculating the accumulated time extent of the ECRs, we see that the CLRs cover approximately 40 h of the available plasma sheet data for all three

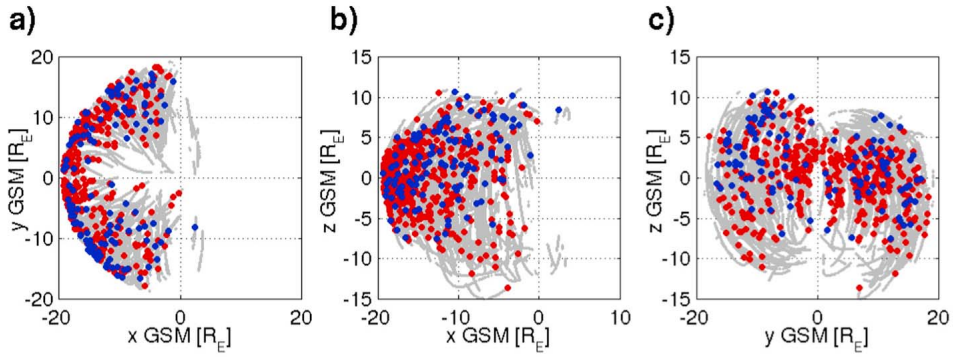

Figure 4. The location of CLRs (red) and CGRs (blue) in the GSM *xy*, *xz*, and *yz* planes. The grey lines indicate where Cluster has been sampling during the summer and fall half-years of 2001, 2002, and 2004, when the spacecraft probed the plasma sheet at geocentric distances of about 15–20R_E.

years together, while CGRs cover only about 6.6 h. Comparing the accumulated time extent of ECRs with the available Cluster plasma sheet data, we see that ECRs are observed about 2% of the time. This can be compared with earthward moving BBFs, which are dominantly observed for $x_{GSM} \lesssim -20R_E$ [e.g., *Baumjohann et al.*, 1990], and which are reported to occur <15% of the time in the plasma sheet at geocentrical distances of 16–22R_E [*Angelopoulos et al.*, 1999]. According to *Baumjohann et al.* [1990] and *Shiokawa et al.* [1997], the occurrence rate decreases toward the Earth due to flow braking. However, it should be noted that the ECR occurrence frequency of ~2% most probably is an underestimate, since we do not claim to select all ECRs existing in the plasma sheet, but only the most distinct ones. Moreover, ECRs and BBFs most likely have different spatial and temporal features, which complicates a detailed comparison of the occurrence frequencies.

[37] For all years, from Table 1 we also see that the ratio between the number of CLRs and the number of CGRs is around three or larger. Since there are more CLRs than CGRs in the database, the statistics for the CLRs is better. Results concerning CLRs are hence likely to be more statistically significant than the results for CGRs.

[38] As discussed by *Hamrin et al.* [2009a, 2010], this observed predomination of CLRs over CGRs (number of events and accumulated time extent) is consistent with the plasma sheet, on the average, behaving as a load. This overall load behavior of the plasma sheet is caused by the cross tail current and the dawn-dusk electric field. On the other hand, the plasma sheet also shows a high level of fine structure, hosting generator regions as well as loads, even though generators are less common. Note that the dominance of load regions over generator regions in the plasma sheet is also visible from the RAND data, where the ratio between the number of RAND-Ls and RAND-Gs is larger than one, even though it is smaller than the corresponding ratio for the ECRs. Since the RAND data are expected to capture the general behavior of the plasma sheet (as well as the background noise and variability level), this is again consistent with the average load behavior of the plasma sheet.

[39] The Cluster scale size, indicated in the last column of Table 1, is typically smaller than the scale size of the ECRs (see section 3.5 and *Hamrin et al.* [2009b]). This renders Cluster as an appropriate platform for investigating ECRs.

3.2. ECR Location

[40] The ECR spatial location was investigated by *Hamrin et al.* [2009a] who used Cluster plasma sheet data from 2001. In this overview article, we return to this issue by using data from all three available years (2001 + 2002 + 2004). Figure 4 shows the location of CLRs (red) and CGRs (blue) in the GSM *xy*, *xz*, and *yz* planes. The grey lines show where Cluster has been probing the plasma sheet. We observe that the ECRs are distributed over the plasma sheet at geocentric distances of about 15–20R_E. However, from the rightmost plot we see that there is a tendency of CLRs appearing closer to the central plasma sheet, while CGRs prefer locations further out, possibly toward the PSBL. This is consistent with previous investigation by *Hamrin et al.* [2009a] and *Marghitu et al.* [2010]. Our results are also supported by large-scale MHD simulations of *Birn and Hesse* [2005], which show that the plasma sheet is highly structured on smaller scales, and with generator regions generally existing closer to the PSBL. In the simulation by *Birn and Hesse* [2005], generator regions are found off the equatorial plane.

[41] Without complementary data (or detailed investigations of all individual events), from Figure 4 it is not possible to draw more precise conclusions about the ECR location. The reason is the general plasma sheet motion, thinning, and expansion during the substorm cycle. Further information on the ECR location with respect to the central plasma sheet and the PSBL can, however, be obtained by including data of variations in the magnetic field (as was done by *Hamrin et al.* [2009a]), or by using the plasma β, i.e., the ratio between the plasma pressure and the magnetic pressure. In this present article we use the plasma β to further investigate the ECR location. Note that we assume that the electron pressure makes just a minor contribution, and therefore only use the ion pressure in the calculation of β. For example, according to *Baumjohann et al.* [1989], it has been shown that the ratio between the ion and electron temperatures in the plasma sheet is $5.5 < T_i/T_e < 11$. The ion pressure hence dominates β.

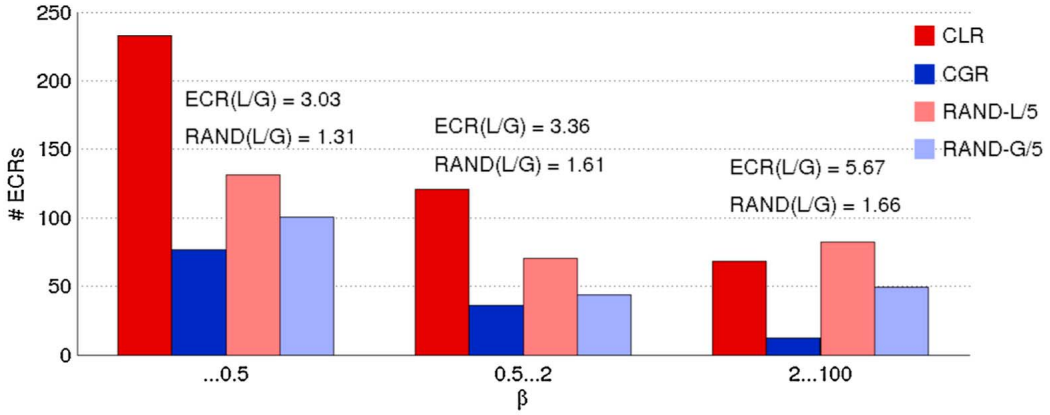

Figure 5. Number of ECR and RAND events for different plasma β values during 2001, 2002, and 2004. From left to right, the three bins correspond to low β events ($\beta < 0.5$), medium β events ($0.5 \leq \beta < 2$), and strong β events ($\beta \geq 2$). Generally, smaller β values correspond to the PSBL, and higher β values correspond to the central plasma sheet [*Baumjohann et al.*, 1988, 1989]. Red and blue colors are used to indicate CLRs and CGRs, respectively, while light red and light blue are reserved for RAND-Ls and RAND-Gs. Note that the number of RAND events is divided by five, to fit into the diagrams. For each β bin, the ratio between the number of CLRs and CGRs, as well as between the number of RAND-Ls and RAND-Gs, is also indicated.

[42] Figure 5 shows the ECR occurrence frequency versus plasma β for the summer and fall half-years of 2001, 2002, and 2004. The events are binned into three intervals corresponding to low β, medium β, and high β values, respectively. The ratio between the number of load and generator regions (both CLRs/CGRs and RAND-Ls/RAND-Gs) is also presented in the diagram.

[43] According to *Baumjohann et al.* [1988, 1989], the ion β approaches small values in the PSBL, of the order of $\beta \lesssim 0.1$, while the central plasma sheet corresponds to higher values, $\beta \gtrsim 0.1$. From Figure 5, we clearly see that the ratio between the number of CLRs and the number of CGRs is considerably larger in the rightmost bin (high β bin) as compared to the leftmost bin (low β bin). ECR(C/L)=3.03 for the leftmost bin, and 5.67 for the rightmost bin, i.e., corresponding to CLRs preferring locations toward the central plasma sheet, as compared to CGRs, which appear closer to the PSBL in a lower β plasma. The ratio is substantially larger for true ECRs (CLRs/CGRs) than for the background RAND events (RAND-Ls/RAND-Gs), and we therefore believe that the result is significant for the ECRs observed in the plasma sheet at Cluster altitudes.

[44] According to detailed analysis of the data (not shown) we note that Cluster probes the low β plasma ($\beta < 0.5$) in the plasma sheet approximately equally often as the medium and high β plasma together ($0.5 < \beta < 2$ and $\beta \geq 2$) during the three years of interest. The histogram in Figure 5 has not been normalized against this variation in the Cluster plasma sheet coverage between the bins. However, this variation in the coverage does not influence the ratio between the number of loads and generators within each bin. Moreover, Figure 5 has not been corrected for variations due to instrumental degradings over the years, which cause a slight decreasing trend of the observed β (not shown). Consequently, using the same bin limits for all included years, as in Figure 5, is not optimal. However, detailed analysis of the data (not shown) indicates that the general conclusion is not altered by changing the bin limits. We hence we note that the main result is not dependent on the details of the binning, and we conclude that there is an increased probability of observing CLRs during high β, i.e., toward the central plasma sheet. Similarly, CGRs are more generally observed during low β, i.e., toward the PSBL. This is consistent with the GSM *yz* distribution presented in Figure 4.

3.3. ECR Strength

[45] In Figure 6, we show the power density strength of the energy conversion regions by using data from 2001, 2002, and 2004. In previous investigations, only data from 2001 were used [*Hamrin et al.*, 2009a]. The strength is estimated by the step value (see Figure 3), which corresponds to the total amount of energy converted by the ECRs. Both effects from a higher average power density within the event, as well as a longer lifetime of the event, are included in the step value. From Figure 6, we see that CLRs are stronger and converts more energy than CGRs. This is again consistent with previous investigations [*Hamrin et al.*, 2009a], and with the notion of the plasma sheet, on the average, behaving as a load. Note that the colored bars (average value) generally are larger than the white bars (median value). This implies the existence of strong ECRs, which increase the average value as compared to the median.

[46] There is considerably more energy converted within CLRs and CGRs, than within the background plasma sheet, as estimated from the data of RAND-Ls and RAND-Gs. However, among the RAND data there is also a trend of load regions being stronger than generator region, i.e., RAND-Ls being stronger than RAND-Gs.

[47] According to previous investigations [*Hamrin et al.*, 2006, 2009a], the GSM cross-tail E_yJ_y component gives the dominant contribution to the total power density, $\mathbf{E} \cdot \mathbf{J} = E_xJ_x + E_yJ_y + E_zJ_z$. The z direction occasionally contributes significantly to the total power density, while the E_xJ_x contribution generally is the smallest one. This is true for both CLRs and CGRs.

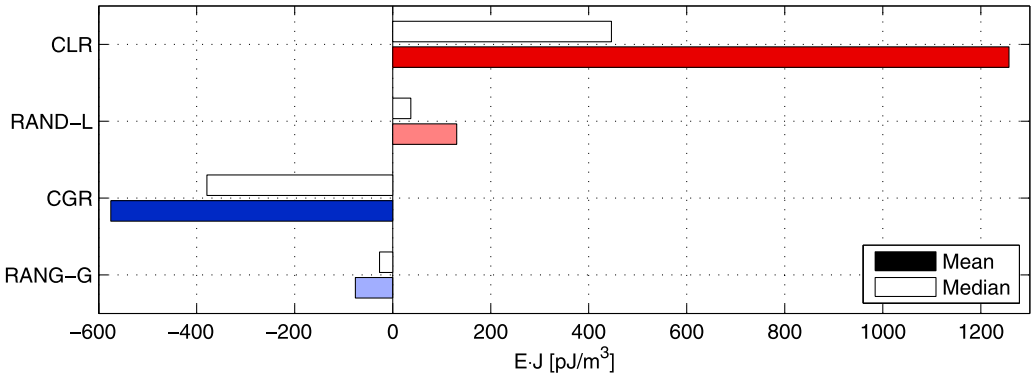

Figure 6. Strength of ECR and RAND events using the step size of the accumulated power density (time integration along the spacecraft path, see Figure 3). This estimate corresponds to the total amount of energy converted by the ECRs. Data from 2001, 2002, and 2004 are used. Red and light red correspond to CLRs and RAND-Ls, while blue and light blue correspond to CGRs and RAND-Gs. Both median (white bars) and mean (colored bars) values are presented.

[48] In a simple magnetic field configuration in the equatorial plane (as in Figure 2), a major contribution from the y direction to the ECR power density would be consistent with plasma dominantly flowing toward or away from the Earth. However, note that ECRs are observed both in the CPS and in the PSBL, and more complicated magnetic field configurations are generally expected. Therefore more detailed investigations of the observed plasma flows are of course needed to reveal the relation between BBFs and ECRs. Previous investigations by *Hamrin et al.*, [2009] have shown that CLRs often have $E_y > 0$ and $J_y > 0$, while for CGRs the situation is less clear, even though there is a slight dominance of $E_y < 0$ and $J_y > 0$. In a simplified magnetotail configuration, we would hence expect that CLRs more often correlate with earthward flows, while for CGRs, tailward plasma flows (e.g., BBF return flows) may as well be important for the energy conversion.

[49] In summary, as shown by the higher CLR occurrence frequency and the stronger CLR power density, the dominance of CLRs over CGRs (see sections 3.1 and 3.3) is consistent with an overall load behavior of the plasma sheet energy conversion. At the same time, the plasma sheet also shows a high level of fine structure both regarding the plasma flow and the energy conversion, with the existence of BBFs, CLRs, and CGRs of variable magnitude and in various regions of the plasma sheet.

3.4. ECR Lifetime

[50] As discussed in relation to Figure 2, magnetic tension and magnetic pressure accelerate and decelerate the plasma, resulting in energy being transferred between its kinetic and electromagnetic forms. It is reasonable to assume that at least some of the energy oscillate back and forth between the fields and particles locally in the plasma sheet, e.g., within and in the neighborhood of BBFs, while some energy is transported away from the local energy conversion regions, e.g., to the ionosphere (see Figure 1). This is consistent with the large-scale MHD simulation by *Birn and Hesse* [2005] who investigated energy release, conversion and transport processes in the magnetotail and plasma sheet, and who showed that the energy conversion (at least in the region of the PSBL) is not time stationary. The power density varies with time at localized regions in space. According to *Birn and Hesse* [2005, Figure 9], the energy conversion oscillates between generator and load character, with periods of the order of 4 min, with generator character during slightly more than half this time interval.

[51] *Hamrin et al.* [2009b] used a database of automatically selected events from 2001 to investigate time and space variations of ECRs in the Cluster plasma sheet data. To separate temporal from spatial variations, they analyzed the local power density observed by each spacecraft. By using the electric field observed by the individual satellites (instead of the electric field averaged over all available satellites, as was used in the other investigations), together with the more global curlometer current density, they obtained an approximate estimate of the local power density.

[52] Using this approximation of the local power density, and assuming that ECRs are some kind of coherent structures, *Hamrin et al.* [2009b] also investigated the propagation of ECRs. As discussed before, it is reasonable to expect that ECRs and BBFs are related, and that ECRs corresponds to regions where the plasma is accelerated or decelerated by the magnetic pressure and tension. According to the simplified picture in Figure 2, one possibility is that CGRs (CLRs) move together with the front (rear) side of the BBF. Another possibility (see Figure 2) is that CLRs and CGRs are associated with the central and the return flow channels, respectively. Further investigations are needed before we know the details of the propagation of the ECRs in relation to the plasma flow and the BBFs. However, *Hamrin et al.* [2009b] showed that it is likely that most of the analyzed plasma sheet ECRs are rather stationary in space. Only a minority of the events were found to propagate across the spacecraft, resulting in an observed time shift between the local power density obtained by the individual satellites. In general, the local power density increases almost simultaneously on all spacecraft (see *Hamrin et al.* [2009b, Figure 3] for some examples of power density signatures observed by the different spacecraft).

[53] Since the maximum time resolution of ion moments from CODIF is 4 s, time shifts shorter than this are impossible to resolve in the available data. By using the characteristic scale size of the Cluster tetrahedron (see Table 1)

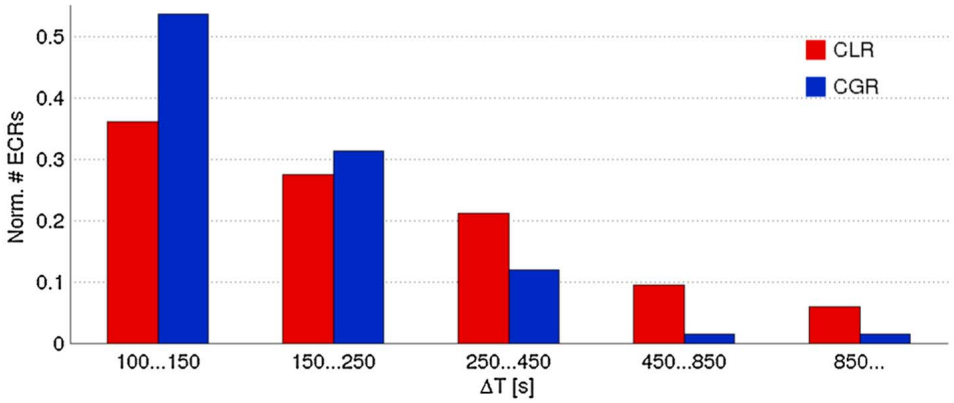

Figure 7. Lifetime of CLRs (red) and CGRs (blue). The data are normalized so that the CLR bars sum up to one and similar for the CGR bars. The lower cutoff at 100 s is caused by the event selection criterion, which accepts no events shorter than 100 s.

as a proxy for the spacecraft separation, this maximum time resolution can be translated into a velocity threshold for the observable ECR propagation velocity. In 2001, the size of the tetrahedron was about 1500 km, implying that only ECR propagation speeds $\lesssim$400 km/s can be analyzed. For the data from 2002, the corresponding requirement would be $\lesssim$1000 km/s. If the ECRs are propagating with a higher velocity, a corresponding time shift would not be possible to resolve. From a manual inspection of all events included in the database, as well as from a detailed analysis of the cross-correlation coefficient, *Hamrin et al.* [2009b] concluded that a majority of the ECRs observed in the Cluster plasma sheet data in 2001 is not associated with time shifts $\gtrsim$4 s. The observed time extent of the ECRs in 2001 should therefore be interpreted as an estimate of their lifetime, instead of an indication of their propagation in space. Note that using data from 2003 one could also investigate the possibility of ECRs propagating with a higher velocity. However, this is outside the scope of the present article.

[54] Using Cluster data from 2001, *Hamrin et al.* [2009b] showed that the ECR lifetime is of the order of 1–10 min, with CLRs having a slightly larger lifetime than CGRs. The result is reproduced in Figure 7 by using a larger database including plasma sheet ECRs from both 2001 and 2004 when the Cluster tetrahedron size was very similar (see Table 1). According to above, this implies similar thresholds for resolving the velocity of the ECRs. No extra manual inspection has, however, been performed on the 2004 data. The data are normalized so that the number of CLRs sums to one over the bins, and similar for the CGRs. The cutoff at 100 s is caused by the automatic selection routine, which does not accept shorter events since they may be highly affected by noise. A short event, only containing a few 4 s samples of the power density (see section 2), can easily be misinterpreted as a true ECRs due to the probability of observing a small number of consecutive (noisy or random) power density values with the same sign. From Figure 7 we see that the ECR occurrence frequency increases toward smaller ΔT, with an average ΔT of about 1–10 min. Even though we cannot analyze events shorter than 100 s, there is a tendency of the histogram bars increasing toward and below 100 s, i.e., indicating the existence of shorter events. Since the CGR bars in Figure 7 increase faster toward small ΔT, we also conclude that the lifetime of CGRs is shorter than for the CLRs.

[55] An ECR lifetime of 1–10 min is of the same order as the estimate obtained from the MHD simulation presented by *Birn and Hesse* [2005]. Indeed, it is noteworthy that similar results are obtained from the two investigations. *Hamrin et al.* [2009b] studied an approximate cross section of the plasma sheet at Cluster altitudes by using observational data from several Cluster passages. *Birn and Hesse* [2005], on the other hand, used a large-scale MHD simulation for investigating power density variations at a specific location in space (close to the PSBL), and within a confined period of time (the first ~20 min of the simulation).

[56] The possible relation between BBFs and ECRs in the plasma sheet can be explored further by comparing their respective time durations. By using Cluster data, *Cao et al.* [2006] and *Juusola et al.* [2009] showed that the average duration of BBFs in the plasma sheet is approximately 3–20 min. This is consistent with the 1–10 min lifetime reported by *Hamrin et al.* [2009b].

[57] As discussed above, it is reasonable to assume that energy is converted back and forth between its kinetic and electromagnetic forms in plasma sheet CLRs and CGRs. However, the observed difference in occurrence frequency and strength between CLRs and CGRs (see sections 3.1 and 3.3) does not agree with simple (harmonic) oscillations back and forth in the plasma sheet energy conversion between $\mathbf{E} \cdot \mathbf{J} > 0$ and $\mathbf{E} \cdot \mathbf{J} < 0$. Comparing with results from the simulation presented by *Birn and Hesse* [2005], the power density does indeed oscillate, but not symmetrically. In fact, load regions appear to be somewhat weaker and shorter than generator regions. According to *Birn and Hesse* [2005], generator regions extend over longer times (~140 s) than load regions (~100 s). Though, as mentioned before, the simulation by *Birn and Hesse* [2005] corresponds to regions close to the PSBL, whereas the observational investigations instead concern a larger region of the plasma sheet, including both the PSBL and regions closer to the neutral sheet. An exact agreement between the two investigations is therefore not to be expected. Instead it should be noted that the simulation confirms the observational con-

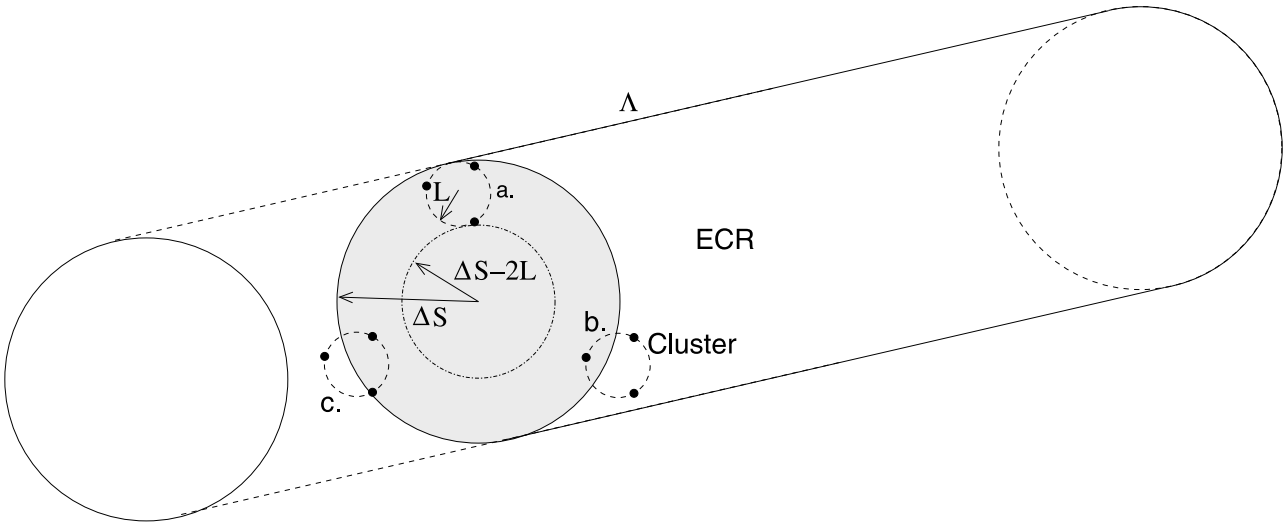

Figure 8. Three examples of the Cluster spacecraft overlapping the cross section of an assumed cylindrical ECR. L is the characteristic size of the Cluster tetrahedron, and ΔS is the radius of the ECR cylinder [from *Hamrin et al.*, 2009b].

clusions of energy oscillating back and forth, with the appearance of CLRs and CGRs of nonequal power density strength and lifetime.

3.5. ECR Scale Size

[58] Based on the assumption that the ECRs in general do not propagate across the Cluster path, but instead grow and decay in more localized regions in space, we can estimate the scale size of the ECRs. If the power density is largest at the center of an ECR, and decreasing toward its boundary, it is possible to resolve each satellite's closeness to the ECR edge by analyzing the variation in power density between the satellites. *Hamrin et al.* [2009b] used Cluster plasma sheet data from 2001 to manually identify those events where at least one spacecraft is outside the ECRs.

[59] Using the simple assumption that all ECRs are cylindrically shaped and of equal size, from the statistical distribution of the Cluster spacecraft C1, C3, and C4 (CIS is not operational on C2) over the observed ECRs, the ECR scale size can be estimated. Figure 8 shows the cross section of a cylindrical ECR together with three different examples of overlapping Cluster spacecraft. Note that the cross section between the Cluster plane and the ECR cylinder generally is an ellipse, if the plane is not normal to the cylinder axis. According to Figure 8, the probability of observing all spacecraft inside an ECR is

$$P = \frac{(\Delta S - 2L)^2}{\Delta S^2}, \tag{5}$$

where L is the scale size of the Cluster tetrahedron, and ΔS is the radius of the cross section of the cylindrical ECR. Solving for ΔS from equation (3), *Hamrin et al.* [2009b] used Cluster plasma sheet data from 2001 to obtain an approximate scale size of the ECRs according to $3R_E \lesssim \Delta S_{CLR} \lesssim 8R_E$ and $1R_E \lesssim \Delta S_{CGR} \lesssim 3R_E$ for CLRs and CGRs, respectively. From Figure 4, we see that the cross-section dimension of the plasma sheet at Cluster altitudes is of the order of 20–40R_E. The observed ECRs hence occupy a significant part of the plasma sheet.

[60] Comparing the ECR and BBF scale sizes, observational investigations have confirmed that BBFs are narrow and elongated structures, whose cross-tail scale size is of the order of 1 or a few R_E [e.g., *Sergeev et al.*, 1996a; *Angelopoulos et al.*, 1997; *Nakamura et al.*, 2004, 2005a; *Walsh et al.*, 2009]. *Walsh et al.* [2009] estimated that the BBF size along the direction of the plasma flow is approximately ~4R_E. This is of the same order as the estimated ECR scale size, strengthening the assumption that ECRs and BBFs are intimately related. *Nakamura et al.* [2005a] suggested that the width of the BBFs is smaller in the north–south direction than in the dawn-dusk direction. However, according to above, we have only calculated a rough estimate of the ECR scale size, assuming an elongated cylindrical shape, but neglecting any variation between the north–south and dawn-dusk directions. Hence, a detailed comparison between the ECR and BBF dimensions is not possible at present. In the previous investigation by *Hamrin et al.* [2009b], the orientation of the assumed cylinder axis was not directly discussed. However, comparing the ECRs with observations of BBFs, a probable orientation is approximately along GSM x. Depending on which plasma sheet regime is under consideration (CPS or PSBL), the axis orientation should vary between (quasi-) perpendicular and (quasi-) parallel to the magnetic field. The BBFs are dominantly (quasi-) perpendicular to the magnetic field in the CPS [*Angelopoulos et al.*, 1994], and they are likely to extend into field-aligned beams in the PSBL [*Nakamura et al.*, 1992; *Petrukovich et al.*, 2001].

4. Dependence on Magnetospheric Activity

[61] Using the Kp index as a proxy for the geomagnetic activity, *Hamrin et al.* [2010] showed that the energy conversion in the plasma sheet ECRs observed in 2001, 2002, and 2004 increases with increasing geomagnetic activity. The Kp index [*Bartels et al.*, 1939] is a quasi-logarithmic index measuring the planetary activity level, and it ranges between 0 and 9. Finer variations are indicated by minus and

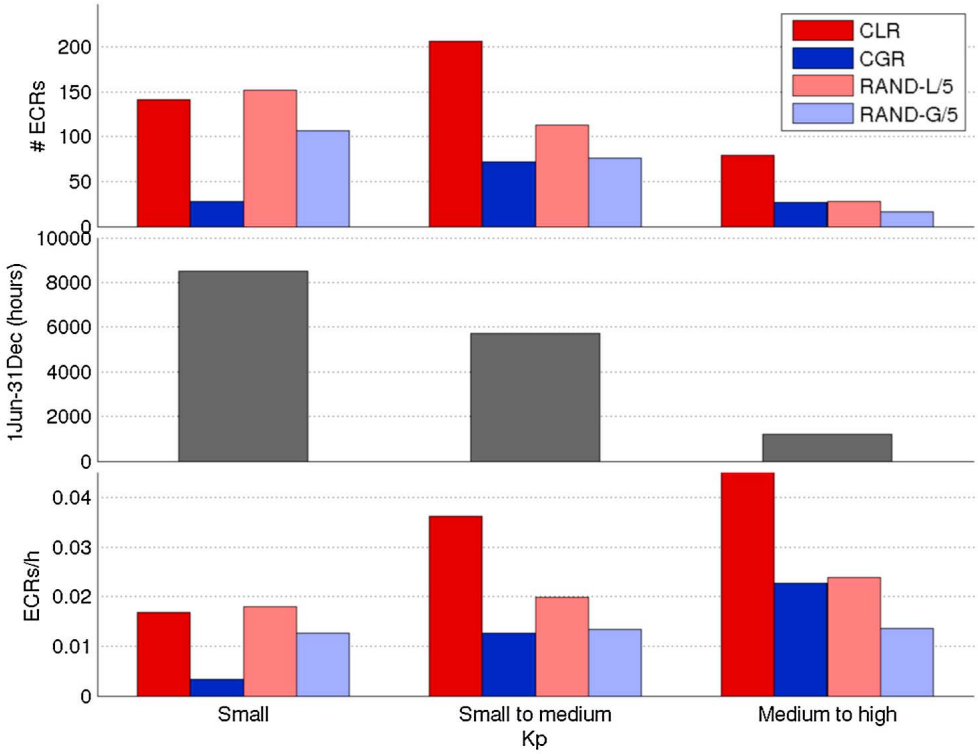

Figure 9. ECRs and RAND events versus Kp. The three bins correspond to $0 \leq Kp \leq 2$, $2+ \leq Kp \leq 4$, and $4+ \leq Kp \leq 9+$. (top) The number of CLRs (red), CGRs (blue), RAND-Ls (light red), and RAND-Gs (light blue). (middle) The number of hours of available Kp data within each bin during the second half-years of 2001, 2002, and 2004. This corresponds to the normal Kp variation during the years of interest. (bottom) The number of ECRs and RAND events per hour, and it is obtained by dividing the data in Figure 9 (top) by the data in Figure 9 (bottom) [from *Hamrin et al.*, 2010].

plus signs, e.g., 0, and 0+ designating very quiet magnetospheric conditions, and 9−, 9, and 9+ very disturbed conditions.

[62] Figure 9 shows the occurrence frequency of ECRs and RAND events versus Kp. The data are divided into three bins according to low Kp ($0 \leq Kp \leq 2$), medium Kp ($2+ \leq Kp \leq 4$), and medium to high Kp ($4+ \leq Kp \leq 9+$). Figure 9 (top) shows the number of events within each bin. The normal Kp variation of the plasma sheet is presented in Figure 9 (middle), which contains the total number of hours of available β data within the bins during the second half-years of 2001, 2002, and 2004. Dividing the data in Figure 9 (top and middle), we obtain the number of events per hour, as presented in Figure 9 (bottom).

[63] From Figure 9 (bottom), we see that the occurrence frequency of both CLRs and CGRs increases with increasing magnetospheric activity as measured by Kp. *Hamrin et al.* [2010] also investigated the variation of the ECR power density strength (as measured by the average power density, see Figure 3), as well as the variation of the ECR lifetime, as a function of Kp. The power density strength of both CLRs and CGRs was found to increase with increasing Kp (not shown). Considering the lifetime, on the other hand, only CLRs appear to be significantly affected by the geomagnetic activity as measured by the Kp index, with the CLR lifetime increasing with increasing Kp.

[64] In addition to analyzing the Kp dependence, *Hamrin et al.* [2010] also studied ECR variations with AE and Dst. The AE index measures the auroral electrojet [*Davis and Sugiura*, 1966], and the Dst index measures variations in the ring current [*Akasofu and Chapman*, 1964]. *Hamrin et al.* [2010] observed that plasma sheet energy conversion is influenced similarly by the geomagnetic activity as measured by variations in Kp and AE. The occurrence frequency and power density strength increase with increasing Kp and AE, both for CLRs and CGRs, but an increase in lifetime was only noted for the CLRs. As for the ECR variations with Dst, the signatures were less clear, even though a measurable increase in occurrence frequency was observed also for increasing Dst. This is consistent with BBFs which are believed to have an increased occurrence during times of higher geomagnetic activity as measured by the AE index [e.g., *Baumjohann et al.*, 1990; *Angelopoulos et al.*, 1994].

[65] Energy conversion hence increases rather simultaneously with increasing geomagnetic activity, both in CLRs and CGRs. This indicates a relationship between energy conversion in the Cluster plasma sheet in both directions between the particles and the electromagnetic field, i.e., between the kinetic and electromagnetic energy forms. Energy conversion in load regions appears not to operate independently of the generators, and vice versa, even though the picture of course is complicated by energy also being transported away, e.g., to the ionosphere.

[66] The stronger response in the plasma sheet energy conversion toward variations in AE and Kp, than toward variations in Dst, is consistent with the plasma sheet magnetically mapping to the auroral zone, and reflects a tighter correlation between the plasma sheet and the auroral ionosphere, than to the ring current.

5. Explicit Relation to Auroral Activity

[67] Some aspects concerning the relation between ECRs and auroral activity were already discussed in section 4 through the use of the AE index. To further investigate the relation between the observed ECRs and auroral activity at lower altitudes, *Hamrin et al.* [2006] and *Marghitu et al.* [2006] used conjugate FAST and Cluster data for analyzing four CGRs. The CGRs were manually selected from the Cluster power density data from 19–20 September 2001.

[68] Figure 10 shows some overview Cluster and FAST data for these CGRs, which are highlighted in yellow. The conjugation times are indicated with the vertical magenta lines. Figures 10a–10f contain Cluster data according to: HIA proton energy, FGM magnetic field, current density, CIS electric field, accumulated power density, and field-aligned Poynting flux. The accumulated power density is obtained as a cumulative sum along the spacecraft path.

[69] To be comparable with the current density, which inherently is an average through the computation of $\nabla \times \mathbf{B}$, the magnetic and electric fields in Figures 10b and 10d are averaged over the Cluster spacecraft. The power density and the Poynting flux in Figures 10e and 10f are consequently also obtained as averages over the Cluster spacecraft. In earlier investigations, the electric field average was performed over available COD measurements on C1, C3, and C4 [*Hamrin et al.*, 2006; *Marghitu et al.*, 2006, 2010; *Hamrin et al.*, 2009a, 2009b]. In recent investigations and in Figure 10d, COD on C3 has been removed from the average due to a degraded particle detection efficiency (see section 2), and measurements from HIA on C1 and C3 have been included [*Hamrin et al.*, 2010]. The solid black lines in Figures 10e and 10f correspond to the earlier average (only COD included), and the green lines to the recent average (both COD and HIA). Independently of the method of averaging, we see that the CGR signature of $\mathbf{E} \cdot \mathbf{J} < 0$ is still present, even though the absolute value of the accumulated power density varies (note the different scales of the black and green axes in Figure 10e).

[70] A slowly sloping trend is observed in Figure 10e, both in the COD (black) and the COD+HIA (green) estimates of the accumulated power density, but the total falloff during the entire observation time is larger for the COD estimate. Even though this slowly sloping trend most likely is artificial, in general we cannot entirely exclude the possible existence of more extended ECRs in the plasma sheet. However, for the investigations reviewed in this article, we have only focused on more concentrated ECRs.

[71] The black dashed line in Figure 10e is the E_yJ_y contribution using the EFW electric field in a satellite coordinate system almost parallel to GSM y. Note that the dashed line closely follows the variations of the solid lines, indicating a consistency between the CIS and EFW observations, as well as a dominance of the y contribution to the total power density.

[72] As can be seen from the data presented by *Hamrin et al.* [2006] and *Marghitu et al.* [2006], at least some of CGRs discussed in this article are observed in relation to rather high-speed plasma flows of $\gtrsim$100 km/s. This again strengthens the assumption that there is a relationship between CGRs and BBFs.

[73] The CGRs observed on 19–20 September 2001, are rather weak as compared to the power density of the events included in the database of automatically identified ECRs from 2001 [*Hamrin et al.*, 2009a], as well as from 2002 and 2004 [*Hamrin et al.*, 2010]. However, requiring conjunction between Cluster and FAST at the time of the ECRs is a practical limitation for the event selection.

[74] The Cluster-FAST conjunctions discussed by *Hamrin et al.* [2006] and *Marghitu et al.* [2006] are indicated by the vertical magenta lines in Figure 10. The field line mapping between Cluster and FAST is based on the Tsyganenko T96 model, which is complicated due to the fact that Cluster is close to apogee at high altitudes. However, the geomagnetic activity is low (Kp = 1), making the mapping more reliable. Moreover, similar particle data signatures on FAST and Cluster support the mapping. For the three conjunctions, the ionospheric footprints of Cluster and FAST meet almost head-on, with FAST moving eastward at almost constant latitudes, while the footprints of Cluster follow a declined path equatorward toward local midnight.

[75] Corresponding FAST electron data are presented in Figures 10g–10i. To reflect the almost head-on encounter of the mapped ionospheric footprints of Cluster and FAST, note that the time axes have been reversed for the FAST data. As can be seen from the electron energy and pitch angle spectrograms in Figures 10g and 10h, there is evidence for accelerated auroral electrons with loss cone distributions approximately at 22:22:30–22:23:30, 00:24–00:28, and 00:36–00:38, i.e., around the conjunction times. Inspecting Figure 10, we see that the first and third conjunctions occur just after Cluster has observed a CGR, while the second

Figure 10. Conjugated Cluster (Figures 10a–10f) and FAST (Figures 10g–10i) data for the four CGRs observed on 19–20 September 2001. The CGRs are highlighted in yellow, and the conjugation times are indicated by the vertical magenta lines. (a) HIA proton energy spectrograms from C1 and (b) GSE x, y, and z components of the FGM magnetic field averaged over C1, C3, and C4. (c) GSE x, y, and z components of the current density. (d) GSE x, y, and z components of the electric field averaged over available HIA and CIS measurement on C1, C3, and C4. (e) Accumulated power density obtained as a cumulative sum along the spacecraft path. The solid lines correspond to averages over C1, C3, and C4 using COD data only (black line) and both COD and HIA data (green line). The dashed black line is the E_yJ_y contribution using the EFW electric field in a satellite coordinate system almost parallel to GSM y. Note the different scales of the axes. (f) Field-aligned Poynting flux (using the electric field averaged over available HIA and CIS measurement on C1, C3, and C4). (g–i) FAST electron energy spectrogram, pitch angle spectrograms, and electron energy flux observed around the conjugation times. Note that the time axes have been reversed for the FAST data.

conjunction occurs a while before the third CGR. However, as mentioned above, the FAST and Cluster footprints meet approximately head-on. For the third CGR, this implies that FAST has recently left an inverted-V region, while Cluster is approaching a CGR.

[76] Hence, even though the magnetic field line mapping is somewhat uncertain due to the large distance between FAST and Cluster, we believe that the data support the interpretation that these CGRs observed by Cluster in the plasma sheet on 19–20 September 2001, indeed are related

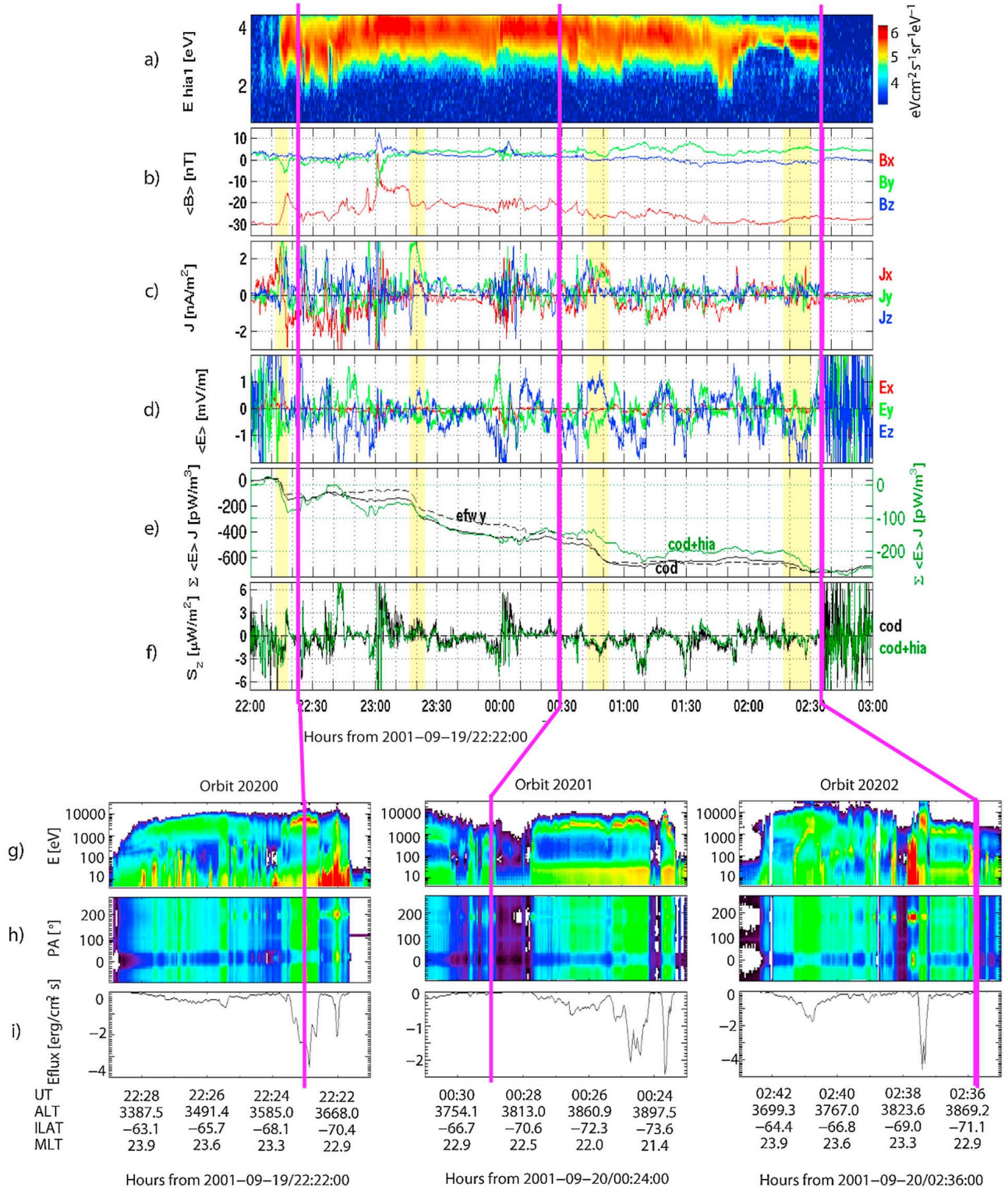

Figure 10

to auroral activity at lower altitudes. The field-aligned Poynting flux in Figure 10f is dominantly directed toward the Earth during three of the CGRs. Figure 10i shows the electron energy flux observed by FAST. Mapping the observed downward Poynting flux at Cluster altitudes [c.f. *Hamrin et al.*, 2006] to the FAST altitude, we obtain a value of about 2 mW/m^2 (or 2 $erg/cm^2\ s^{-1}$), which is comparable to the FAST energy flux observed within the inverted-V regions.

[77] To further investigate a possible relation to auroral activity, *Hamrin et al.* [2010] used Cluster plasma sheet data from 2001, 2002, and 2004 to study the influence on the ECRs from variations in the AE (Auroral Electrojet) index. Note that the AE index is designed to measure auroral activity by capturing the behavior of the auroral electrojet [*Davis and Sugiura*, 1966]. *Hamrin et al.* [2010] showed that the occurrence frequency, as well as the power density strength, of both CLRs and CGRs increase during times of high AE [see *Hamrin et al.*, 2010, Figures 3 and 6a]. Moreover, the lifetime of the CLRs increases with increasing AE. Using the AE index as a proxy for auroral activity, we can hence conclude that there indeed is some relation between auroral activity and the energy conversion in the plasma sheet, even at geocentric distances of 15–20R_E. This increased plasma sheet energy conversion apparently involves both CLRs and CGRs, and it corresponds to a higher level of energy conversion back and forth between electromagnetic and kinetic energy forms.

[78] However, we do not claim that all ECRs observed in the Cluster plasma sheet data are directly connected to auroral activity at lower altitudes. For example, according to the data presented by *Hamrin et al.* [2010], there are also ECRs which are observed during periods of low AE, and which cannot be expected to be directly related to auroras. Moreover, preliminary investigations show that the plasma sheet energy conversion at Cluster altitudes only responds weakly to variations in the ionization (as estimated by the F10.7 index) at the ionospheric end of the auroral current circuit. Assuming that the ionospheric feedback mechanism [*Atkinson*, 1970; *Sato*, 1978; *Lysak*, 1991] affects the M-I coupling, auroral acceleration should be more efficient when the ionospheric conductivity is low. If there were a strong correlation between auroral activity and the observed ECRs, the plasma sheet energy conversion at Cluster altitudes would also vary substantially with the ionospheric ionization.

6. Summary and Conclusions

[79] In this article we have reviewed a set of investigations using Cluster data from the summer and fall half-years of 2001, 2002, and 2004 for analyzing energy conversion in the plasma sheet at altitudes of 15–20R_E. Transfer from electromagnetic energy to kinetic energy occurs in load regions where the power density is positive, $\mathbf{E} \cdot \mathbf{J} > 0$. The process is reversed in generator regions where $\mathbf{E} \cdot \mathbf{J} < 0$. From the Cluster data, approximately three times as many CLRs as CGRs are identified, and the CLRs appear to be stronger than the CGRs. This predominance of CLRs over CGRs is consistent with the plasma sheet, on the average, behaving as a load due to the large-scale cross-tail current and dawn-dusk electric field. On smaller scales, on the other hand, the plasma sheet power density shows a high level of fine structure. The scale size and lifetime of the ECRs are observed to be a few R_E and a few minutes, respectively. At least some of the ECRs appear to be related to auroral activity.

[80] The plasma sheet energy conversion increases with increasing geomagnetic activity in both CLRs and CGRs, indicating a correlated rate of activity of the energy conversion in both directions between electromagnetic and kinetic energy forms. It is possible that ECRs rise and vanish locally in significant regions of the plasma sheet, oscillating between load and generator character, even though the picture is complicated by the fact that some energy most likely is transmitted as Poynting flux toward the ionospheres.

[81] As discussed in this article, there are reasons to expect that there is a tight relationship between ECRs and BBFs in the plasma sheet, even though more thorough investigations are needed before we understand the detailed relationship between ECRs and BBFs. While ECRs are relevant for the energy conversion between the electromagnetic field and the particles, BBFs play a central role in plasma and energy transfer in the plasma sheet. Indeed, in this article we have shown that general properties of ECRs and BBFs are similar. For example, both the scale size and lifetime of ECRs and BBFs are comparable, and they show a similar dependence on the geomagnetic activity.

[82] **Acknowledgments.** We thank the FGM, CIS, and EFW teams for providing magnetic field, ion, and electric field data from Cluster. We also thank the FAST team for the conjugate low-altitude data. O.M. acknowledges support through the PECS contract ECSTRA, C98048. We thank K. Rönnmark for fruitful discussions. We thank our referees for thoroughly reviewing our manuscript.

[83] Robert Lysak thanks the reviewers for their assistance in evaluating this paper.

References

Akasofu, S., and S. Chapman (1964), On the asymmetric development of magnetic storm fields in low and middle latitudes, *Planet. Space Sci.*, *12*, 607–636, doi:10.1016/0032-0633(64)90008-X.

Angelopoulos, V., W. Baumjohann, C. F. Kennel, F. V. Coroniti, M. G. Kivelson, R. Pellat, R. J. Walker, H. Lühr, and G. Paschmann (1992), Bursty bulk flows in the inner central plasma sheet, *J. Geophys. Res.*, *97*(A4), 4027–4039.

Angelopoulos, V., C. F. Kennel, F. V. Coroniti, R. Pellat, M. G. Kivelson, R. J. Walker, C. T. Russell, W. Baumjohann, W. C. Feldman, and J. T. Gosling (1994), Statistical characteristics of bursty bulk flow events, *J. Geophys. Res.*, *99*(A11), 21,257–21,280.

Angelopoulos, V., et al. (1997), Magnetotail flow bursts: Association to global magnetospheric circulation, relationship to ionospheric activity and direct evidence for localization, *Geophys. Res. Lett.*, *24*(18), 2271–2274.

Angelopoulos, V., F. S. Mozer, R. P. Lin, T. Mukai, K. Tsuruda, R. Lepping, and W. Baumjohann (1999), Comment on "Geotail survey of ion flow in the plasma sheet: Observations between 10 and 50 R-E" by W. R. Paterson et al., *J. Geophys. Res.*, *104*(A8), 17,521–17,525.

Angelopoulos, V., J. A. Chapman, F. S. Mozer, J. D. Scudder, C. T. Russell, K. Tsuruda, T. Mukai, T. J. Hughes, and K. Yumoto (2002), Plasma sheet electromagnetic power generation and its dissipation along auroral field lines, *J. Geophys. Res.*, *107*(A8), 1181, doi:10.1029/2001JA900136.

Atkinson, G. (1970), Auroral arcs: Result of interaction of a dynamic magnetosphere with ionosphere, *J. Geophys. Res.*, *75*(25), 4746–4766.

Barger, V. D., and M. G. Olsson (1987), *Classical Electricity and Magnetism: A Contemporary Perspective*, Allyn and Bacon, Boston, Mass.

Bartels, J., N. H. Heck, and H. F. Johnston (1939), The three-hour index measuring geomagnetic activity, *Terr. Magn. Atmos. Electr.*, *44*(4), 411–454.

Baumjohann, W., G. Paschmann, N. Sckopke, C. A. Cattell, and C. W. Carlson (1988), Average ion moments in the plasma sheet boundary-layer, *J. Geophys. Res.*, *93*(A10), 11,507–11,520.

Baumjohann, W., G. Paschmann, and C. A. Cattell (1989), Average plasma properties in the central plasma sheet, *J. Geophys. Res.*, *94*(A6), 6597–6606.
Baumjohann, W., G. Paschmann, and H. Lühr (1990), Characteristics of high-speed ion flows in the plasma sheet, *J. Geophys. Res.*, *95*(A4), 3801–3809.
Birn, J., and M. Hesse (1996), Details of current disruption and diversion in simulations of magnetotail dynamics, *J. Geophys. Res.*, *101*(A7), 15,345–15,358.
Birn, J., and M. Hesse (2005), Energy release and conversion by reconnection in the magnetotail, *Ann. Geophys.*, *23*, 3365–3373.
Birn, J., M. Hesse, G. Haerendel, W. Baumjohann, and K. Shiokawa (1999), Flow braking and the substorm current wedge, *J. Geophys. Res.*, *104*(A9), 19,895–19,903.
Birn, J., J. Raeder, Y. L. Wang, R. A. Wolf, and M. Hesse (2004), On the propagation of bubbles in the geomagnetic tail, *Ann. Geophys.*, *22*, 1773–1786.
Birn, J., R. Nakamura, E. V. Panov, and M. Hesse (2011), Bursty bulk flows and dipolarization in MHD simulations of magnetotail reconnection, *J. Geophys. Res.*, *116*, A01210, doi:10.1029/2010JA016083.
Cao, J. B., et al. (2006), Joint observations by Cluster satellites of bursty bulk flows in the magnetotail, *J. Geophys. Res.*, *111*, A04206, doi:10.1029/2005JA011322.
Chen, C. X., and R. A. Wolf (1993), Interpretation of high-speed flows in the plasma sheet, *J. Geophys. Res.*, *98*(A12), 21,409–21,419.
Chen, C. X., and R. A. Wolf (1999), Theory of thin-filament motion in Earth's magnetotail and its application to bursty bulk flows, *J. Geophys. Res.*, *104*(A7), 14,613–14,626.
Davis, T. N., and M. Sugiura (1966), Auroral electrojet activity index AE and its universal time variations, *J. Geophys. Res.*, *71*(3), 785–801.
Dungey, J. (1961), Interplanetary magnetic field and auroral zones, *Phys. Rev. Lett.*, *6*(2), 47–48.
Dunlop, M. W., A. Balogh, K. H. Glassmeier, and P. Robert (2002), Four-point Cluster application of magnetic field analysis tools: The Curlometer, *J. Geophys. Res.*, *107*(A11), 1384, doi:10.1029/2001JA005088.
Escoubet, C. P., M. Fehringer, and M. Goldstein (2001), The Cluster mission, *Ann. Geophys.*, *19*, 1195–1200.
Fairfield, D., et al. (1999), Earthward flow bursts in the inner magnetotail and their relation to auroral brightenings, AKR intensifications, geosynchronous particle injections and magnetic activity, *J. Geophys. Res.*, *104*(A1), 355–370.
Forsyth, C., et al. (2008), Observed tail current systems associated with bursty bulk flows and auroral streamers during a period of multiple substorms, *Ann. Geophys.*, *26*, 167–184.
Fujimoto, M., T. Nagai, N. Yokokawa, Y. Yamade, T. Mukai, Y. Saito, and S. Kokubun (2001), Tailward electrons at the lobe-plasma sheet interface detected upon dipolarizations, *J. Geophys. Res.*, *106*(A10), 21,255–21,262.
Ge, Y. S., J. Raeder, V. Angelopoulos, M. L. Gilson, and A. Runov (2011), Interaction of dipolarization fronts within multiple bursty bulk flows in global MHD simulations of a substorm on 27 February 2009, *J. Geophys. Res.*, *116*, A00I23, doi:10.1029/2010JA015758.
Hamrin, M., O. Marghitu, K. Rönnmark, B. Klecker, M. André, S. Buchert, L. M. Kistler, J. McFadden, H. Rème, and A. Vaivads (2006), Observations of concentrated generator regions in the nightside magnetosphere by Cluster/FAST conjunctions, *Ann. Geophys.*, *24*, 637–649.
Hamrin, M., P. Norqvist, O. Marghitu, S. Buchert, B. Klecker, L. M. Kistler, and I. Dandouras (2009a), Occurrence and location of concentrated load and generator regions observed by Cluster in the plasma sheet, *Ann. Geophys.*, *27*, 4131–4146.
Hamrin, M., P. Norqvist, O. Marghitu, A. Vaivads, B. Klecker, L. M. Kistler, and I. Dandouras (2009b), Scale size and life time of energy conversion regions observed by Cluster in the plasma sheet, *Ann. Geophys.*, *27*, 4147–4155.
Hamrin, M., P. Norqvist, O. Marghitu, S. Buchert, B. Klecker, L. M. Kistler, and I. Dandouras (2010), Geomagnetic activity effects on plasma sheet energy conversion, *Ann. Geophys.*, *28*, 1813–1825.
Ieda, A., S. Machida, T. Mukai, Y. Saito, T. Yamamoto, A. Nishida, T. Terasawa, and S. Kokubun (1998), Statistical analysis of the plasmoid evolution with Geotail observations, *J. Geophys. Res.*, *103*(A3), 4453–4466.
Ieda, A., D. H. Fairfield, T. Mukai, Y. Saito, S. Kokubun, K. Liou, C.-I. Meng, G. K. Parks, and M. J. Brittnacher (2001), Plasmoid ejection and auroral brightenings, *J. Geophys. Res.*, *106*(A3), 3845–3857.
Juusola, L., R. Nakamura, O. Amm, and K. Kauristie (2009), Conjugate ionospheric equivalent currents during bursty bulk flows, *J. Geophys. Res.*, *114*, A04313, doi:10.1029/2008JA013908.
Kauristie, K., V. A. Sergeev, M. Kubyshkina, T. I. Pulkkinen, V. Angelopoulos, T. Phan, R. P. Lin, and J. A. Slavin (2000), Ionospheric current signatures of transient plasma sheet flows, *J. Geophys. Res.*, *105*(A5), 10,677–10,690.
Keiling, A., et al. (2009), Substorm current wedge driven by plasma flow vortices: THEMIS observations, *J. Geophys. Res.*, *114*, A00C22, doi:10.1029/2009JA014114.
Koskinen, H. E. J., and E. I. Tanskanen (2002), Magnetospheric energy budget and the epsilon parameter, *J. Geophys. Res.*, *107*(A11), 1415, doi:10.1029/2002JA009283.
Lyons, L. R., T. Nagai, G. T. Blanchard, J. C. Samson, T. Yamamoto, T. Mukai, A. Nishida, and S. Kokubun (1999), Association between Geotail plasma flows and auroral poleward boundary intensifications observed by CANOPUS photometers, *J. Geophys. Res.*, *104*(A3), 4485–4500.
Lyons, L. R. (2000), Geomagnetic disturbances: Characteristics of, distinction between types, and relations to interplanetary conditions, *J. Atmos. Terr. Phys.*, *62*(12), 1087–1114, doi:10.1016/S1364-6826(00)00097-3.
Lysak, R. L. (1991), Feedback instability of the ionospheric resonant cavity, *J. Geophys. Res.*, *96*(A2), 1553–1568.
Marghitu, O., M. Hamrin, B. Klcecker, A. Vaivads, J. McFadden, S. Buchert, L. M. Kistler, I. Dandouras, M. André, and H. Rème (2006), Experimental investigation of auroral generator regions with conjugate Cluster and FAST data, *Ann. Geophys.*, *24*, 619–635.
Marghitu, O., M. Hamrin, B. Klecker, K. Rönnmark, S. Buchert, L. M. Kistler, M. André, and H. Rème (2010), Cluster observations of energy conversion regions in the plasma sheet, in *The Cluster Active Archive*, edited by H. Laasko et al., pp. 453–459, Springer, New York, doi:10.1007/978-90-481-3499-132.
Mauk, B., B. Anderson, and R. Thorne (2002), Magnetosphere-ionosphere coupling at Earth, Jupiter, and beyond, in *Atmospheres in the Solar System: Comparative Aeronomy*, *Geophys. Monogr. Ser.*, vol. 130, edited by M. Mendillo, A. Nagy, and J. H. Waite, pp. 97–114, AGU, Washington, D. C.
Miyashita, Y., S. Machida, K. Liou, T. Mukai, Y. Saito, C. Meng, and G. Parks (2003), Relationship between magnetotail variations and auroral activities during substorms, *J. Geophys. Res.*, *108*(A1), 1022, doi:10.1029/2001JA009175.
Morioka, A., et al. (2010), Two-step evolution of auroral acceleration at substorm onset, *J. Geophys. Res.*, *115*, A11213, doi:10.1029/2010JA015361.
Nagai, T., I. Shinohara, M. Fujimoto, M. Hoshino, Y. Saito, S. Machida, and T. Mukai (2001), Geotail observations of the Hall current system: Evidence of magnetic reconnection in the magnetotail, *J. Geophys. Res.*, *106*(A11), 25,929–25,949.
Nakamura, M., G. Paschmann, W. Baumjohann, and N. Sckopke (1992), Ion distributions and flows in and near the plasma sheet boundary-layer, *J. Geophys. Res.*, *97*(A2), 1449–1460.
Nakamura, R., W. Baumjohann, M. Brittnacher, V. Sergeev, M. Kubyshkina, T. Mukai, and K. Liou (2001a), Flow bursts and auroral activations: Onset timing and foot point location, *J. Geophys. Res.*, *106*(A6), 10,777–10,789.
Nakamura, R., W. Baumjohann, R. Schodel, M. Brittnacher, V. Sergeev, M. Kubyshkina, T. Mukai, and K. Liou (2001b), Earthward flow bursts, auroral streamers, and small expansions, *J. Geophys. Res.*, *106*(A6), 10,791–10,802.
Nakamura, R., et al. (2004), Spatial scale of high-speed flows in the plasma sheet observed by Cluster, *Geophys. Res. Lett.*, *31*, L09804 doi:10.1029/2004GL019558.
Nakamura, R., et al. (2005a), Multi-point observation of the high-speed flows in the plasma sheet, *Adv. Space Res.*, *36*(8), 1444–1447, doi:10.1016/j.asr.2005.05.101.
Nakamura, R., et al. (2005b), Localized fast flow disturbance observed in the plasma sheet and in the ionosphere, *Ann. Geophys.*, *23*, 553–566.
Ohtani, S., Y. Miyashita, H. Singer, and T. Mukai (2009), Tailward flows with positive B-Z in the near-Earth plasma sheet, *J. Geophys. Res.*, *114*, A06218, doi:10.1029/2009JA014159.
Panov, E. V., et al. (2010a), Multiple overshoot and rebound of a bursty bulk flow, *Geophys. Res. Lett.*, *37*, L08103, doi:10.1029/2009GL041971.
Panov, E. V., et al. (2010b), Plasma sheet thickness during a bursty bulk flow reversal, *J. Geophys. Res.*, *115*, A05213, doi:10.1029/2009JA014743.
Paschmann, G. (2008), Recent in-situ observations of magnetic reconnection in near-Earth space, *Geophys. Res. Lett.*, *35*, L19109, doi:10.1029/2008GL035297.
Paschmann, G., B. U. Ö. Sonnerup, I. Papamastorakis, N. Sckopke, G. Haerendel, S. J. Bame, J. R. Asbridge, J. T. Gosling, C. T. Russell, and R. C. Elphic (1979), Plasma acceleration at the earths magnetopause: Evidence for reconnection, *Nature*, *282*(5736), 243–246.
Petrukovich, A., W. Baumjohann, R. Nakamura, R. Schodel, and T. Mukai (2001), Are earthward bursty bulk flows convective or field-aligned?, *J. Geophys. Res.*, *106*(A10), 21,211–21,215.
Pitkänen, T., A. T. Aikio, O. Amm, K. Kauristie, H. Nilsson, and K. U. Kaila (2011), EISCAT-Cluster observations of quiet-time near-Earth

magnetotail fast flows and their signatures in the ionosphere, *Ann. Geophys.*, *29*, 299–319.
Pontius, D. H., and R. A. Wolf (1990), Transient flux tubes in the terrestrial magnetosphere, *Geophys. Res. Lett.*, *17*(1), 49–52.
Pulkkinen, T. I., E. I. Tanskanen, M. Wiltberger, J. A. Slavin, T. Nagai, G. D. Reeves, L. A. Frank, and J. B. Sigwarth (2003), Magnetotail flows can consume as much solar wind energy as a substorm, *J. Geophys. Res.*, *108*(A8), 1326, doi:10.1029/2001JA009132.
Raj, A., T. Phan, R. Lin, and V. Angelopoulos (2002), Wind survey of high-speed bulk flows and field-aligned beams in the near-Earth plasma sheet, *J. Geophys. Res.*, *107*(A12), 1419, doi:10.1029/2001JA007547.
Robert, P., M. W. Dunlop, A. Roux, and G. Chanteur (1998), Accuracy of current density determination, in *Analysis Methods for Multi-Spacecraft Data*, edited by G. Paschmann and P. W. Daly, *Rep. SR-001*, Int. Space Sci. Inst., Bern.
Rosenqvist, L., S. Buchert, H. Opgenoorth, A. Vaivads, and G. Lu (2006), Magnetospheric energy budget during huge geomagnetic activity using Cluster and ground-based data, *J. Geophys. Res.*, *111*, A10211, doi:10.1029/2006JA011608.
Rostoker, G. (1999), The evolving concept of a magnetospheric substorm, *J. Atmos. Terr. Phys.*, *61*(1–2), 85–100.
Sato, T. (1978), Theory of quiet auroral arcs, *J. Geophys. Res.*, *83*(A3), 1042–1048.
Schödel, R., W. Baumjohann, R. Nakamura, V. Sergeev, and T. Mukai (2001), Rapid flux transport in the central plasma sheet, *J. Geophys. Res.*, *106*(A1), 301–313.
Scholer, M., B. Klecker, D. Hovestadt, G. Gloeckler, F. M. Ipavich, and E. J. Smith (1984), Fast moving plasma structures in the distant magnetotail, *J. Geophys. Res.*, *89*(A8), 6717–6727.
Sergeev, V. (2004), Bursty bulk flows and their ionospheric footprints, in *Multiscale Processes in the Earth's Magnetosphere: From Interball to Cluster*, *NATO Sci. Ser., II*, vol. 178, edited by J. A. Sauvaud, and Z. Němeček, pp. 289–306, Kluwer Acad., Boston, Mass.
Sergeev, V., V. Angelopoulos, J. Gosling, C. Cattell, and C. Russell (1996a), Detection of localized, plasma-depleted flux tubes or bubbles in the midtail plasma sheet, *J. Geophys. Res.*, *101*(A5), 10,817–10,826.
Sergeev, V., R. Pellinen, and T. Pulkkinen (1996b), Steady magnetospheric convection: A review of recent results, *Space Sci. Rev.*, *75*(3–4), 551–604.
Sergeev, V., M. Kubyshkina, K. Liou, P. Newell, G. Parks, R. Nakamura, and T. Mukai (2001), Substorm and convection bay compared: Auroral and magnetotail dynamics during convection bay, *J. Geophys. Res.*, *106*(A9), 18,843–18,855.
Sharma, A. S., et al. (2008), Transient and localized processes in the magnetotail: A review, *Ann. Geophys.*, *26*, 955–1006.
Shiokawa, K., W. Baumjohann, and G. Haerendel (1997), Braking of high-speed flows in the near-Earth tail, *Geophys. Res. Lett.*, *24*(10), 1179–1182.
Sitnov, M. I., P. N. Guzdar, and M. Swisdak (2005), On the formation of a plasma bubble, *Geophys. Res. Lett.*, *32*, L16103, doi:10.1029/2005GL023585.
Slavin, J. A., M. F. Smith, E. L. Mazur, D. N. Baker, E. W. Hones Jr., T. Iyemori, and E. W. Greenstadt (1993), ISEE 3 observations of traveling compression regions in the Earth's magnetotail, *J. Geophys. Res.*, *98*(A9), 15,425–15,446.
Snekvik, K., et al. (2007), Cluster observations of a field aligned current at the dawn flank of a bursty bulk flow, *Ann. Geophys.*, *25*, 1405–1415.
Treumann, R. A., C. H. Jaroschek, and R. Pottelette (2009), Auroral evidence for multiple reconnection in the magnetospheric tail plasma sheet, *Europhys. Lett.*, *85*(4), doi:10.1209/0295-5075/85/49001.
Walsh, A. P., et al. (2009), Cluster and Double Star multipoint observations of a plasma bubble, *Ann. Geophys.*, *27*, 725–743.
Wygant, J., et al. (2000), Polar spacecraft based comparisons of intense electric fields and Poynting flux near and within the plasma sheet-tail lobe boundary to UVI images: An energy source for the aurora, *J. Geophys. Res.*, *105*(A8), 18,675–18,692.
YuDuan, M., C. JinBin, H. Reme, I. Dandouras, E. Lucek, and M. Dunlop (2010), The radial evolution of earthward BBFs during substorm, *Sci. China-Earth Sci.*, *53*(10), 1542–1551, doi:10.1007/s11430-010-4040-x.
Zhang, J.-C., R. A. Wolf, R. W. Spiro, G. M. Erickson, S. Sazykin, F. R. Toffoletto, and J. Yang (2009), Rice Convection Model simulation of the substorm-associated injection of an observed plasma bubble into the inner magnetosphere: 2. Simulation results, *J. Geophys. Res.*, *114*, A08219, doi:10.1029/2009JA014131.
Zhang, X., V. Angelopoulos, A. Runov, X. Zhou, J. Bonnell, J. P. McFadden, D. Larson, and U. Auster (2011), Current carriers near dipolarization fronts in the magnetotail: A THEMIS event study, *J. Geophys. Res.*, *116*, A00I20, doi:10.1029/2010JA015885.

M. André and S. Buchert, Swedish Institute of Space Physics, Box 537, SE-751 21 Uppsala, Sweden. (mats.andre@irfu.se; stephan.buchert@irfu.se)

I. Dandouras, CESR-CNRS, UMR 5187, 9, Av du Colonel Roche, BP 44346, F-31028 Toulouse CEDEX 4, France. (iannis.dandouras@cesr.fr)

M. Hamrin and P. Norqvist, Department of Physics, Umeå University, SE-901 87 Umeå, Sweden. (hamrin@space.umu.se; norqvist@space.umu.se)

L. M. Kistler, Space Science Center, Institute for the Study of Earth, Oceans, and Space, University of New Hampshire, Morse Hall, 8 College Rd., Durham, NH 03824-3525, USA. (lynn.kistler@unh.edu)

B. Klecker, Max-Planck-Institut für Extraterrestrische Physik, Giessenbachstrasse, D-85748 Garching, Germany. (berndt.klecker@mpe.mpg.de)

O. Marghitu, Institute for Space Sciences, P.O. Box MG-23, RO-77125 Bucharest-Magurele, Romania.